Unravelling Drivers of Morphological Change

A Case Study on the Prins Hendrik Sand Dike

M. Berning

22nd of June 2023, Delft

Delft University of Technology

Unravelling Drivers of Morphological Change

A Case Study on the Prins Hendrik Sand Dike

By

M. Berning

in partial fulfilment of the requirements for the degree of

Master of Science

in Civil Engineering

at the Delft University of Technology,

to be defended publicly on Thursday the 29th of June 2023 at 14:00 PM.

An electronic version of this thesis is available at http://repository.tudelft.nl/.

TU Delft

Supervisor:	Ir. M.A. van der Lugt	TU Delft
Thesis comittee:	Dr. Ir. M.A. de Schipper	TU Delft
	Dr. Ir. B.C. van Prooijen	TU Delft

Preface

This thesis is written as the final part within the Master of Hydraulic Engineering at the TU Delft. The subject of research has been chosen within my personal fascination for the natural complexity of coastal systems and morphological development of beaches.

This research is written for civil engineers interested in the development of sheltered beaches and morphological development thereof (Morphology). It is also purposeful for coastal engineers in the design phase of low-energy sandy beaches in tidal environments (Review on model study results). Furthermore, this research will be useful for academic engineers, or soon to be engineers, continuing research into general morphological development of low-energy sandy beaches, or the Prins Hendrik Sand Dike in specific. Lastly, it compiles data retrieved by Jan De Nul, TU Delft and University if Utrecht, creating a foundation for Hoogheemraadschap Hollands Noorderkwartier and Jan de Nul to open the conversation for needed maintenance works in the upcoming years (Review on model study results) (Sub question 2: Morphologic development)

This research can be used for a quick overview of hydrodynamic conditions and morphodynamic development locally observed at the Prins Hendrik Sand Dike. It proposes a simplified model approach to reconstruct local forcing conditions based on wind and water level data. The applicability of frequently-used longshore sediment transport formulae is derived for low-energy beaches, indicating the importance of waves and currents on development of low-energy sandy coasts. Lastly, this research initiates a discussion into the application of the XBeach numerical modelling to predict morphological development. It highlights the importance of carefully chosen assumptions on forcing climate.

Acknowledgements

I would like to thank my supervisors for assisting me throughout the academic process of writing this thesis. First of all, Ir. Marlies van der Lugt. Paradoxically, through the absence during her pregnancy break, she gave me a boost in my independence. I was on my own, finding my way with the necessary up's and downs. Maybe It sounds strange, but after all I am grateful for that period in time. During the period Marlies was present, I enjoyed the supportive attitude and unconditional directness of your feedback during our weekly meetings. I had to get used to it at first but learned to admire your honesty and sincerity, which pushed me to produce meaningful results.

During the absence of Marlies, I had a close contact with Dr. ir. Matthieu de Schipper. Thank you Matthieu for your moral support, especially during the dark days of December. You managed to say the right things to take my mind off the thesis. You were the one that encouraged me to take a break and reflect every once in a while, a piece of advice I certainly will remember. Finally, thank you Dr.ir. Bram van Prooijen for your sincere interest in my findings and your always inspiring outside projective. I enjoyed seeing you at formal meetings, but also during the Hydraulic coffee breaks on the third floor for a light chat.

- Ir. M.A. van de Lugt
- Dr. Ir. M.A. de Schipper
- Dr. Ir. B.C van Prooijen

Furthermore, I would like to thank Pieter van der Gaag and Otti Kievits. Who have been of great support to me within the process of this thesis. Pieter always made time to discuss measuring set-ups and persistently supported me in my preparations for the fieldwork. Unrelated to this thesis, we worked together as a fieldwork team for the river engineering department. Throwing oranges into the Waal and building shelters against never-ending rain are some fieldwork moments I will surely remember. Then there's Otti, the social glue of the entire hydraulic department. She was always there whenever I wanted to reserve a meeting room, sort out financial business, or just to have a nice long talk with. Whether it was about the arrival of your new fridge, or how your eastern weekend had been in the South of Holland, I always enjoyed stepping into the secretariat of hydraulic engineering.

- Pieter van der Gaag
- Otti Kievits

During my thesis I have found a trustful group of supporters enabling me to do the fieldwork during the cold winter months. Friends and family were all called upon, and without hesitation, stood ready to walk a 10k along the Prins Hendrik Sand Dike at 08:00 in the morning with some lukewarm coffee out of a shabby thermos flask. Without you all, this research would not have been possible, I thank you all so much.

- Victor Gallardo Torres
- Sjoerd Berning
- Jelle Berning
- Julia Houtermans
- Bernd Berning
- Marjolijn Brakel

Lastly, I would like to thank all my friends and family that supported me through the entire process. Kept me sane by taking my mind off of the Prins Hendrik Sand Dike which allowed me to sometimes return to society

Contents

Abstract

Flood defense will have to be strengthened all over the world as sea level rise poses great challenges for the safety of coastal settlements. Strengthening traditional hard flood defenses is becoming increasingly more difficult due to limited space in the coastal zone and large costs inflicted with renovation. Adaptive 'soft solutions' pose an alternative as they make use of natural processes that are able to adapt to changing boundary conditions. The Prins Hendrik Sand Dike is a pilot project of such a soft solution placed in front of an existing hard sea dike. The Prins Hendrik Sand Dike is the subject of this research.

This research strives to identify the role of waves, currents, and water levels on morphological development of the Prins Hendrik Sand Dike. Which requires an identification of the morphological development during the 3.5 years of service lifetime. This is followed by a characterization of the forcing climate based on measured on-site data. This knowledge is used to hindcast the full forcing climate during the PHSD lifetime and calculate morphological development. Lastly, a comparison of calculated and observed morphological development reveals suitability of engineering formulae on low-energy beaches.

Results indicate the spit head develops at a faster rate than predicted in model studies. In addition, constant erosion in the form of coastline retreat is observed in a section that serves as primary sea defense. These findings hamper successful development of habitat and possibly decrease the longevity of the sea defense if maintenance is not performed. Furthermore, waves have been determined to be the dominant forcing mechanism resulting in sediment transport and morphological development. In addition, systematic water level changes that occur under specific wave conditions are identified causing increased Northeastward transport of sediment. These findings likely explain discrepancies between the previously modelled and observed morphological development.

Implications of this research contribute to an understanding of the interconnected nature of forcing scenarios at low-energy beaches and can be used to improve modelling efforts of low-energy beaches. Furthermore, it provides a basis for Hoogheemraadschap Noorderkwartier to make decisions on maintenance activities.

1. Introduction

1.1. Motivation

During the Pleistocene, the Netherlands has expanded seaward as a result of delta progradation coinciding with lowering of the mean sea level. During this period, the shallow North Sea facilitated onshore transport of sediment and supplied the Holland coastline with sandy material; the Holland dune system was naturally created. However, since sea levels are currently increasing, natural strengthening of our dune system has stopped, and structural erosion prevails. This has caused the Dutch to continuously battle against the water throughout modern history.

Climate change will pose a series of challenge for low elevated country of the Netherlands. In the upcoming decades this country will have to deal with more extreme weather and an expected sea level rise of 0.20 meters in 2120 (van Alphen et al., 2022). This will cause existing flood defenses to be upgraded in order to fulfill safety requirements in the future. However, maintaining and upgrading hard flood defenses is costly and new strategies will have to be developed to achieve suitable solutions.

Adaptive 'soft solutions' are able to conform to the rising water level. Soft solutions make use of natural processes that are able to adapt to naturally changing boundary conditions. The Prins Hendrik Sand Dike (PHSD) is a pilot project of such a soft solution and therefore the subject of this research. The PHSD is a sand nourishment placed in front of an existing hard sea dike to increase flood safety. A research and data monitoring campaign is attached to the PHSD project. This master thesis is linked to that research campaign and strives to create a better understanding of these types of solutions based on four-years of on-site data.

1.2. Prins Hendrik Sand Dike and surroundings

Technical studies had shown that reinforcing the old Prins Hendrik Dike in the traditional way, according to the applicable standards and design methods, would require a very wide inner berm. This would be at the expense of the agricultural land, buildings, and nature area. Consequently, an alternative has been proposed that provides for reinforcement on the seaward side of the dike, namely the Prins Hendrik Sand Dike.

The Prins Hendrik Sand Dike is a special solution as it strengthens a traditional hard sea defense with an adaptive soft solution (also called 'coastal retrofit'). Many sea dikes will face similar circumstances and will have to be upgraded to fulfill safety standards. Traditional dike reinforcements are costly and impractical solutions. Therefore, the PHSD is a suitable solution representing an efficient dike reinforcement, while creating added value to surrounding landscape and ecology.

The Prins Hendrik Sand Dike consists of a 'safety dune' and an elongated spit. The safety dune is a sandy dune area that has the core functions of strengthening the sea defense. This safety dune is placed directly in front of the existing Prins Hendrik Dike, on top of an existing shoal. The safety dune attaches to existing sea defenses on both Southwest- and the Northeast borders. Furthermore, the sandy nourishment is extended with an elongated sandy spit that is not part of the primary sea defense. This elongated spit shelters a tidal lagoon with a primary function of habitat development. The studied coastline stretches from the primary sea defense at the NIOZ-harbor over the elongated spit towards the spit head (Figure 1.1).

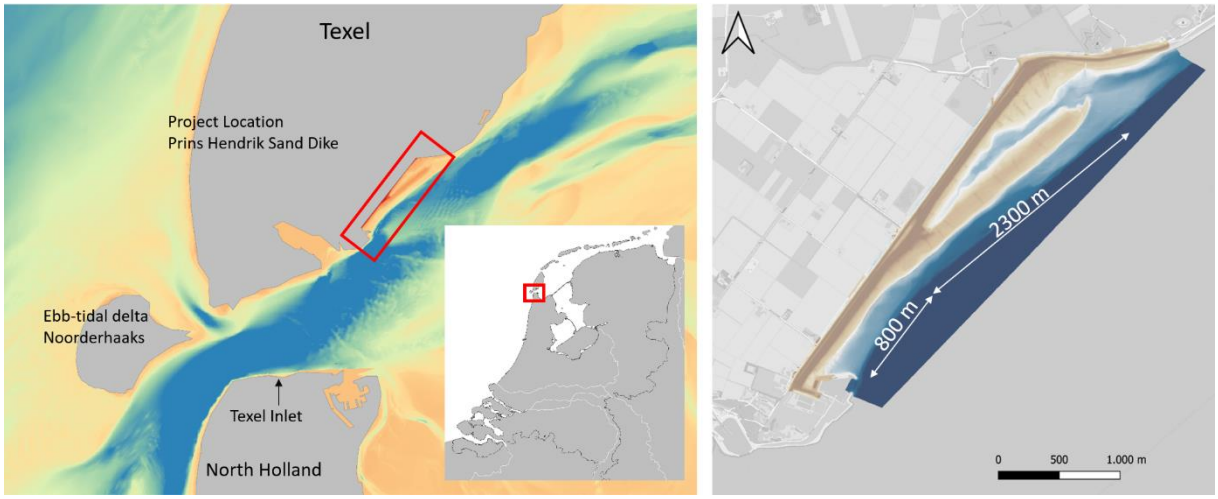

Figure 1.1: The project location is situated on the Southern side of the island Texel, facing the Wadden Sea. Right) Map view of the PHSD based on topographic and bathymetric data from Fall 2020.

1.3. Goal of the research

Morphologic behavior of sand nourishments is generally well-understood on wave-dominated open coast systems (e.g., Sand Motor, Hondsbosche-Pettemer sea defense). However, sand nourishments in sheltered locations, like the Wadden Sea, face more uncertainty, as the interplay of waves, currents, and water levels can have significant influence on sediment transport. This research strives to understand that interplay of waves, currents, and water levels at sheltered beaches based on hydrodynamic data. This uncertainty is also observed in model predictions in the design model study of the PHSD, which underestimated the magnitude and speed at which the spit head develops. The latter is important as it threatens to close off the tidal opening, leading to deterioration of habitat development inside the tidal lagoon, which is one of the required performances of the PHSD. Furthermore, continuous coastal erosion has resulted in a retreat of the coastline in areas that were predicted to be stable. This study also analyses the morphological development of the spit head and compares it to model predictions. This report answers the following main research question.

What is the role of different hydrodynamic forces and how does it influence morphology on the Prins Hendrik Sand Dike?

1.4. Report structure

The research starts with mapping of morphological development based on 3.5 years of data collection during the service lifetime of the PHSD (Morphology). Afterwards, analysis of hydrodynamic data explores the characteristics of the local forcing climate and the interplay of waves, currents, and water levels (Hydrodynamics). This characterization is then used to hindcast the forcing climate on the Prins Hendrik Sand Dike (Hindcasting forcing conditions) and calculate longshore transport (Longshore Transport Approximations). Lastly, the forcing climate is used to approximate longshore sediment transport using engineering formulae, which is compared with morphological development (Discussion). The chapters above create an understanding of morphodynamics on the PHSD, which facilitates the discussion on the accuracy of model results (Witteveen+Bos, 2016).

2. Methodology

This chapter starts with defining the main research question and four sub-research questions. The sub-research questions serve as a guideline throughout this research project and are answered one-by-one in Chapters 3 to 8. Section 2.2 summarizes the methods and data used to answer the sub research questions.

2.1. Research questions

Using the problem analysis, the research questions of this thesis are defined. Under the main research question, a subdivision of the main question into smaller research questions is outlined (Figure 2.1). Left of the sub questions is an overview of the corresponding chapter dedicated to answering that specific question.

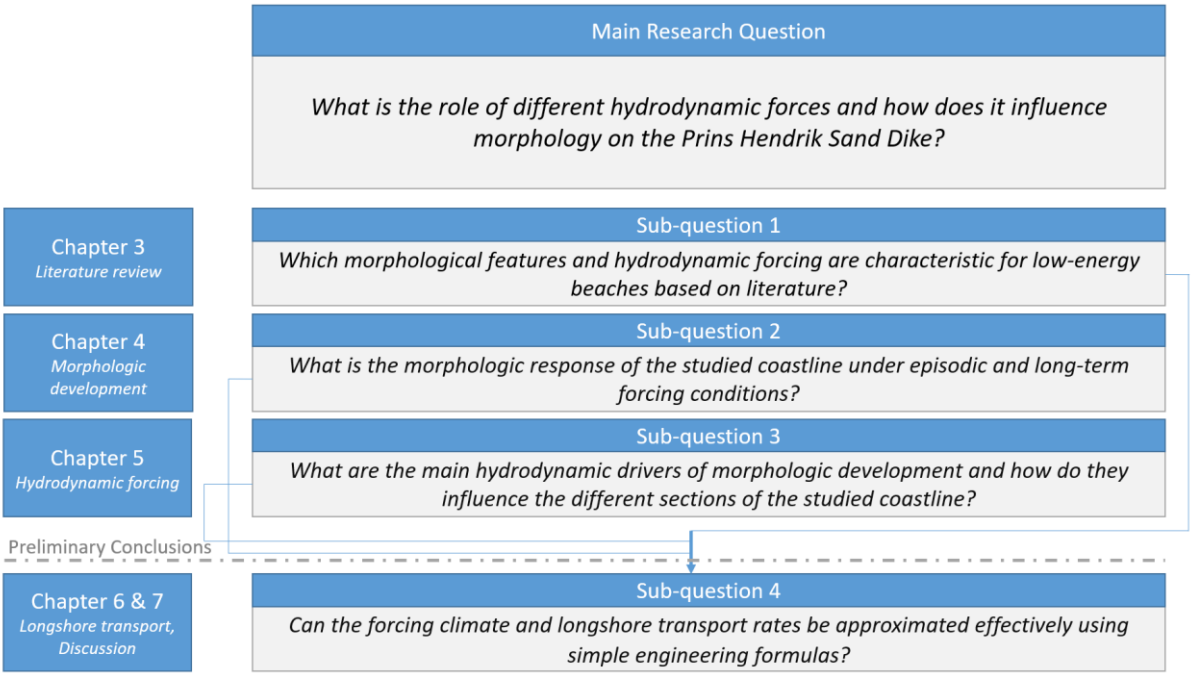

Figure 2.1: Visual overview of main and sub-research questions and corresponding chapters.

2.2. Data overview

The Prins Hendrik Zanddijk has been closely monitored since construction finished in the Fall of 2019. An overview of the different datasets, both previously measured and self-organized, which are used in this research is provided below.

2.2.1. TU Delft and University of Utrecht datasets

EURECCA GPS measurements

Cross-shore transects are measured from dune foot to the deepest accessible point on the low-gradient platform using RTK GNSS GPS measuring. These transects have been walked on a regular basis by the EURECCA team, consisting of Ir. Marlies van der Lugt (TU Delft) and Ir. Jorn van der Bos (UU). Intervals between measurements are two-months on average. Transects are walked on predefined locations on the PHSD from the spit head (L0) to NIOZ harbor (L6). Cross-shore coverage of the low-gradient platform differs depending on local water level conditions, resulting in some measurements to extend to lower depths than others. As the cross-shore profiles are not always walked on the exact same spot due to human error, measurements can include some extra variability. Transects are always reprojected onto the true transect location. This campaign has created a 3.5-year dataset morphological development on the Prins Hendrik Sand Dike.

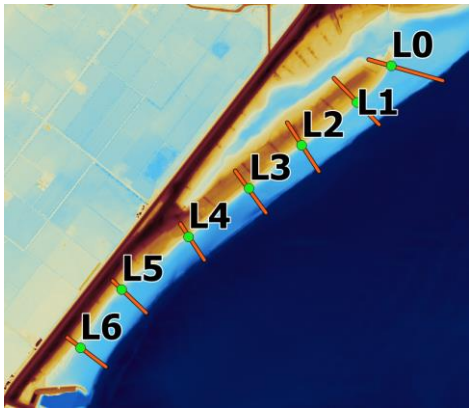

Figure 2.2: Transects measured during the ongoing EURECCA GPS measurement campaign.

SEDMEX campaign

The SEDMEX (mixed SEDiment in Mixed Energy eXperiment) campaign was a combined effort of the TU Delft and the University of Utrecht. It lasted a total of six weeks, starting the 7th of September and ending the 19th of October. A wide variety of instruments was deployed to collect data on local wave and current characteristics as well as profile development and sediment concentrations and grain sizes along the PHSD. Measuring equipment was placed on six arrays from the from spit tip (L1) towards the NIOZ harbour (L6), see the figure below. Confusingly, naming of transects does not correspond to the earlier mentioned GPS campaign. An overview of naming of the transects is elaborated in (Table 2.1).

This Research	GPS campaign	SEDMEX campaign
Transect 0	L0	L1
Transect 1	L1	L2
Transect 2	L2	L3
Transect 3	L3	-
Transect 4	L4	L4
Transect 5	L5	L5
Transect 6	L6	L6

Table 2.1: Table clarifying the naming of the different transects in this research and previous measurement campaigns.

Instrument	Data type	Location of deployment	Sampling frequency
OSSI	Wave	tr0, tr1, tr4, tr5, tr6	10 Hz
ADV	Wave Flow	tr0, tr1, tr2, tr4, tr5, tr6	16 Hz
RTK-GPS	Cross-shore bed elevation	tr0, tr1, tr2, tr4, tr5, tr6	2 days

Table 2.2: Overview of selected set of instruments placed during SEDMEX of which data is used within this research. The placement of instruments and measuring frequency is provided.

A variety of forcing conditions was measured, starting with a relative calm period, followed by a Southwest mild storm, and ending again with calm conditions.

- 9th September - 23rd September: Calm conditions
- 23rd September - 3rd October: Energetic conditions
- 3rd October - 19th October: Calm conditions

2.2.2. Jan de Nul datasets

Jan de Nul has measured the topography on a 3-month interval and bathymetry on yearly intervals. Furthermore, Jan de Nul has deployed an offshore wave buoy twice just offshore of the low-gradient platform in front of transect 3 (Figure 2.3).

Instrument	Data type	Deployment	Duration	Sampling frequency
Xylem Wave buoy	Wave	Offshore (figure 2)	3 months Spring 2021 3 months Fall 2021	Spring 21 Fall 21
LiDAR	Topography	PHSD	Fall 2019 - ongoing	3 months
Multibeam	Bathymetry	PHSD	2019 - ongoing	Yearly

Table 2.3: Overview of measurements campaigns performed by Jan de Nul.

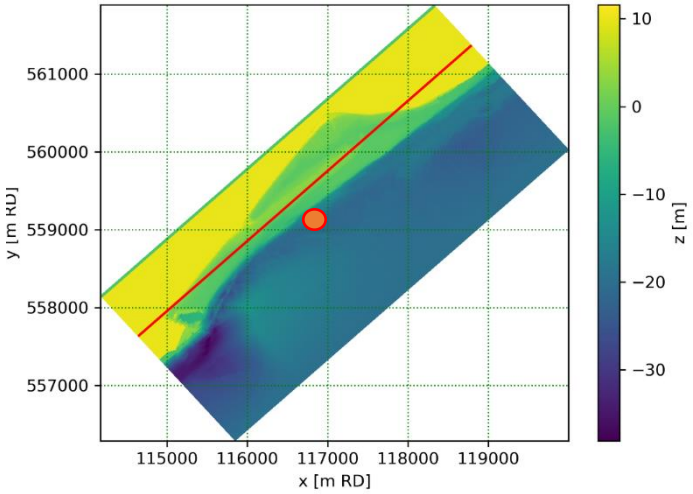

Figure 2.3: Map view of combined topography (LiDAR) and bathymetry (multibeam) measurements from Fall 2019. The offshore xylem wave buoy was deployed offshore at the location of the orange circle.

2.2.3. Continuous datasets

Continuous wind data is retrieved from the KNMI meteorological station 'de Kooij'. This station measures a wide range of meteorological quantities, of which hourly average wind speed and wind direction are used as input for wind wave hindcasts locally at the PHSD (Hindcasting waves). Furthermore, it is often used as supplementary overview of wind forcing conditions accompanying hydrodynamic forcing conditions. The KNMI weather station is located 11 kilometers to the South of the studied coastline

Water level data is retrieved from Rijkswaterstaat water level station at 'Oudeschild'. This long-term dataset is used for an analysis of setup and set-down as a result of wind forcing and is used to transform simulated offshore wind wave conditions to nearshore wind wave conditions. The Rijkswaterstaat Oudeschild water level station is located approximately 4 kilometers Northeast of the PHSD.

Figure 2.4: Map view of the project location (source: Google Maps), with the KNMI weather station and the Rijkswaterstaat water level station indicated.

2.2.4. Self-organized data campaign

HEWO campaign

The HEWO *(High Energy Wave Observations)* campaign is a self-organized data collection campaign aimed to provide an additional nearshore wave dataset within the storm season (December 2022 – March 2023). A longer time series of wave data collected with SOLO wave measurement devices is valuable to perform a more extensive validation of nearshore wave hindcasts (Nearshore waves), as well as the analysis of longshore variation in wave exposure.

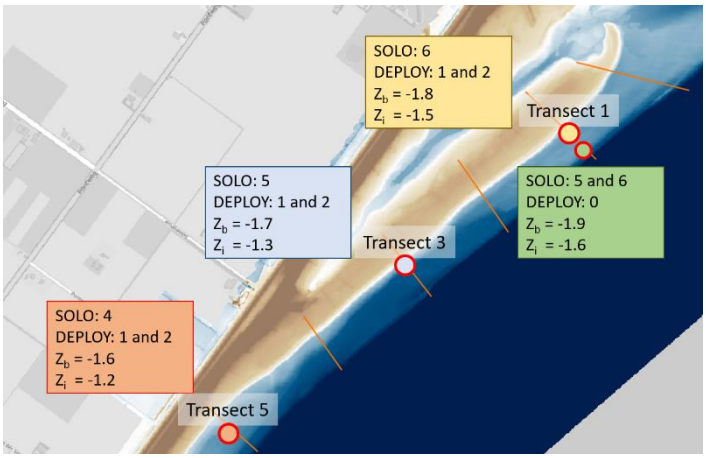

Figure 2.5: Placement of SOLO wave measurement instruments on the PHSD during the HEWO campaign.

	Start Date	End Date	Instruments, measuring frequency	Location of deployment
Deploy 0	03-Dec-2022	17-Dec-2022	SOLO 05, 16Hz SOLO 06, 16HZ	SOLO 05: transect 1 SOLO 06: transect 1
Deploy 1	28-Dec-2022	19-Jan-2023	SOLO 04, 8Hz SOLO 05, 16Hz SOLO 06, 16Hz	SOLO 04: transect 5 SOLO 05: transect 3 SOLO 06: transect 1
Deploy 2	19-Jan-2023	11-Mar-2023	SOLO 04, 8Hz SOLO 05, 8Hz SOLO 06, 8Hz	SOLO 04: transect 5 SOLO 05: transect 3 SOLO 06: transect 1

Table 2.4: Overview of the deployments of SOLO wave instruments during the HEWO campaign and their location.

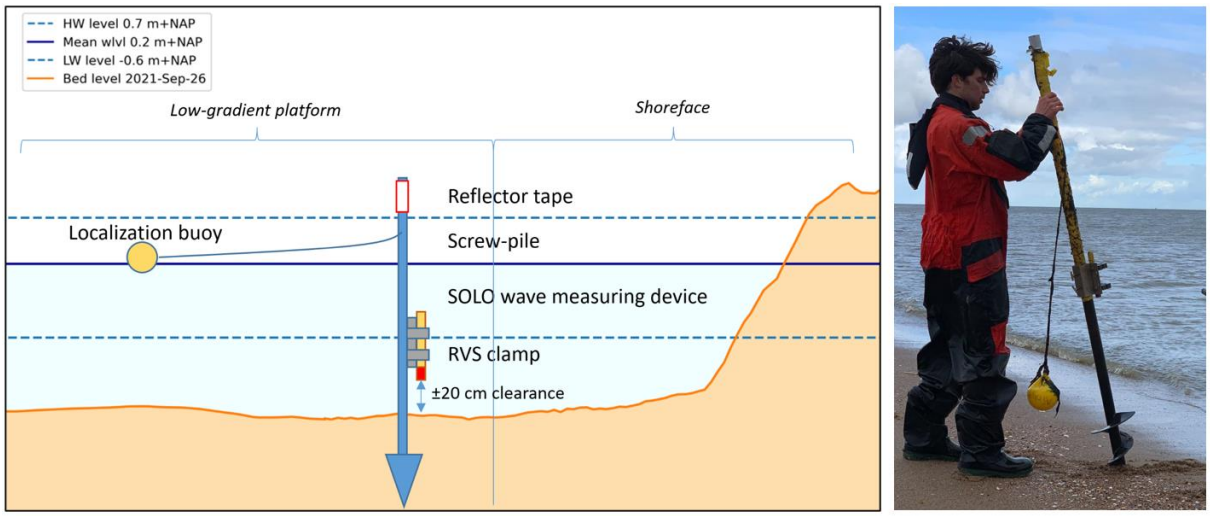

Figure 2.6: Left) Schematized overview of measurement set-up of SOLO wave measuring devices during the HEWO-campaign. Right) picture of retrieved measuring set-up after Deploy 0.

Pop-storm campaign

The POP-Storm *(POst- & Pre-Storm)* campaign is designed to track morphological activity as a result of high energy storm conditions. This campaign facilitates a more detailed study of response to energetic conditions along the studied coastline.

GPS measurements are taken with RTK GNSS GPS equipment on the previously defined transects (transect 0 through transect 6). These measurements contribute to the ongoing EURECCA GPS measurements and add a series of high interval measurements within the storm season. Timing of the GPS measurements is strategically timed with battery changes for SOLO equipment needed within the HEWO campaign.

Below, a summary is provided of all field trips and corresponding on-site activities is provided.

Figure 2.7: Picture of the final field trip on 11th of March indicating the RTK GNSS GPS measurement set-up with walking wheel and handcart for easy transportation of all equipment over the PHSD.

Start date	*End date*	On-site activities
01-Sep-2022	*01-Sep-2022*	GPS measurement (EURECCA)
26-Oct-2022	*26-Oct-2022*	GPS measurement (POP-storm) + assisting Jorn (UU) in collecting sediment samples along the PHSD coastline.
02-Dec-2022	*03-Dec-2022*	GPS measurement (POP-storm) + installing SOLOs before NE storm arrives (HEWO campaign Deploy 0)
17-Dec-2022	*18-Dec-2022*	GPS measurement (POP-storm)
29-Dec-2022	*30-Dec-2022*	GPS measurement (POP-storm) + retrieving SOLOs (HEWO campaign Deploy 0)
23-Jan-2023	*24-Jan-2023*	GPS measurement (POP-storm) and SOLO setup placement (HEWO campaign Deploy 1)
18-Feb-2023	*19-Feb-2023*	GPS measurement (POP-storm) and SOLO setup retrieval (HEWO campaign Deploy 1) and redeployment after battery switch (Deploy 2)
11-Mar-2023	*12-Mar-2023*	GPS measurement (POP-storm) + retrieving SOLOs (HEWO campaign Deploy 2)

Table 2.5: Summary of activities performed per field trip to the Prins Hendrik Sand Dike, Texel.

3. Literature Review

This chapter provides an overview of literature on low energy beaches. Starting with an overview of characteristics of low-energy beaches compared to local properties at the PHSD. Later, a study into forcing of low-energy beaches is presented. The last section focusses on beach morphology and morphodynamic behavior of low-energy beaches.

3.1. Low-energy environments

Low-energy environments have been defined in numerous studies and classification is not consistent throughout, making the term 'low-energy environment' slightly ambiguous. Low-energy beaches occur in a wide range of coastal and estuarine environments. Essential to the term low-energy the absence of high wave-energy. Different degrees of sheltering from adjacent water bodies, by being positioned in a leeward orientation for instance, causes limited wave-energy at low-energy sites (Jackson et al., 2002).

A general criteria list was proposed by (Fellowes et al., 2021) to describe low-energy beaches. This list is added in (Table 3.1) and the properties found at the PHSD are compared. Note that wave conditions and morphological aspects vary depending on the location along the PHSD, therefore, a range of values found on the PHSD is given.

	Range of conditions for low-energy beaches	Prins Hendrik Sand Dike
Non-storm wave heights	$H_s < 0.25$ m	$H_s = 0.05 – 0.12$ m
Significant wave heights during onshore winds	$H_{s,\ onshore} < 0.50$ m	$H_{s,\ onshore} = 0.35$ m
Shoreface width:	20 m (approximately)	20-40 m
Morphologic features include storm relicts	True	True

Table 3.1: Overview of low-energy beach criteria as defined in (Fellowes et al., 2021) *(left) and local measured values on the PHSD (right).*

3.2. Low-energy beach forcing

A brief characterization of the wave climate and the influence of tides and surge is given in this subsection.

3.2.1. Wave climate

Waves in low energy environments can be generated locally or non-locally ((Jackson & Nordstrom, 1992)). Locally generated waves are 'wind waves' and originate from fetch-limited environments such as semi-enclosed basins. Non-locally generated waves are swell waves originating from adjacent water bodies. Swell waves penetrate the low energy environment and can be found near the entrance to the open ocean, in the lee of islands, or behind submerged barriers. Low-energy environments are often fetch-limited and sheltered at the same time; therefore, a mixture of local and non-local waves is often observed.

Locally generated wind waves resulting from fetch-limited environments depend on local wind conditions (speed, direction, and duration) and basin properties (fetch lengths, and depth). The presence of non-locally generated swell waves at low-energy beaches depends on the offshore wave conditions and the configuration of the sheltered area within the surrounding area. Shoreline orientation, distance from entrance, and depth of submerged barriers are all influential factors for swell wave penetration towards low-energy environments.

There are some key differences between wind- and swell waves. Wind waves are generally small (H_s < 0.5 meters) and wave periods are short (T_p< 4.0 seconds). The ability of swell waves to refract towards the shoreline is limited which results in high angles of incidence nearshore, increasing the potential for longshore currents and sediment transport. Swell waves penetrating the low-energy area often have larger wave period and approach the shoreline shore-normal due to refraction. Wave height is often significantly reduced from open ocean conditions due to site specific controls (Jackson et al., 1992).

3.2.2. Influence of tides and surge

The effect of the tide on low-energy beaches is to move different hydrodynamic zones (swash, surf, and shoaling zones) over the cross-shore beach profile. This causes wave energy to become distributed over a certain section of the shoreface as varying water levels cause different zones to become morphologically active throughout the tidal cycle (Jackson et al., 2002).

Under energetic conditions, sediment may be mobilized across the entire profile (foreshore and subaqueous platform) due to increased wave orbital motion. While during calm conditions sediment mobilization and resulting profile change may only be limited to the steep foreshore near the waterline. Since waves are generated by the local wind conditions, transport of sediment on the subaqueous platform may be maximized when strong winds are accompanied by water level set-down.

3.2.3. Sediment transport

Morphological development is a result of net longshore and cross-shore transport of sediment. A conceptual model describing sediment transport on non-tidal low-energy beaches was proposed by (Ton et al., 2021) see (Figure 3.1). Waves approaching the shore cause the steep and narrow shoreface to erode during calm and energetic conditions. Transect measurements indicate simultaneous erosion

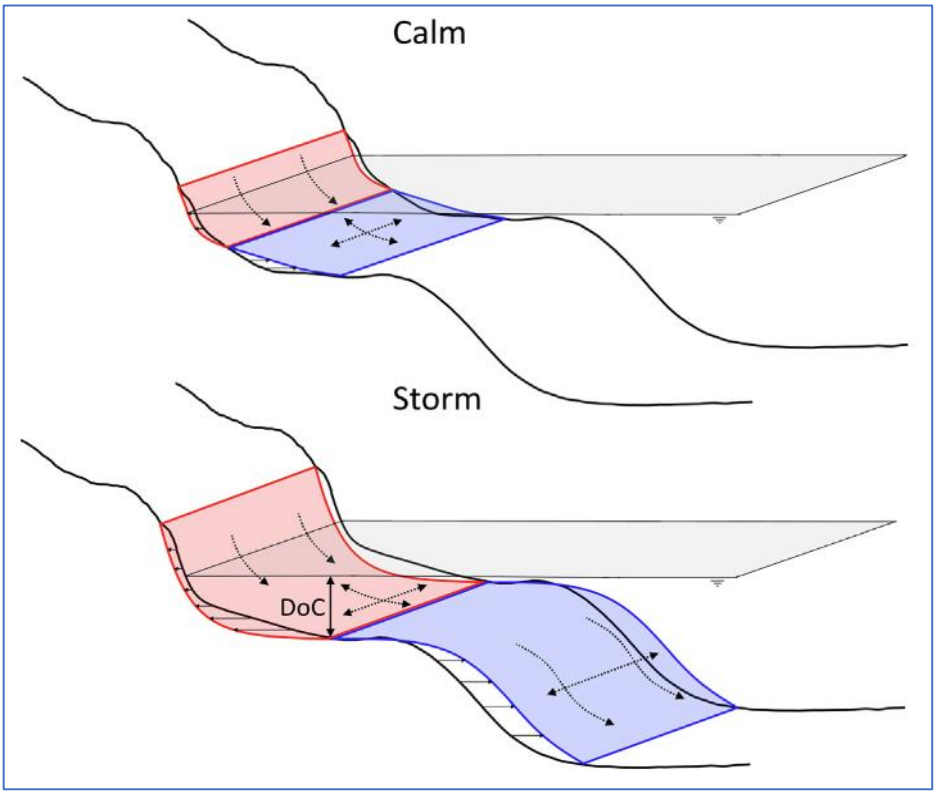

Figure 3.1: A visual summary of the conceptual model for low-energy beach morphodynamics for calm and storm conditions (Ton et al., 2021). *Blue shaded areas indicate accretion and red shaded areas erosion, the dotted arrows indicate possible sediment transport directions.*

of the shoreface and accretion on the low-gradient platform, suggesting sediment transport near the shoreface to be mainly in cross-shore direction during storm conditions. The sediment deposited on the low-gradient platform most-likely travels further in both cross- and longshore directions, to again meet the equilibrium depth. During calm conditions, wave motion does not mobilize sediment and transport is inhibited. In contrast, during more energetic conditions, erosion occurs over the total platform. The magnitude of cross-shore and longshore transports on the platform depends on the combined wave-current bottom shear for sediment mobilization and the prevailing currents driving sediment transport while also determining net transport direction. In addition, post-storm beach recovery on low-energy beaches is often inhibited due to insufficient wave energy for rebuilding during calm conditions in between storms. The latter should be viewed critically in light of the PHSD case study as water levels vary through the tidal cycle, resulting in a less clearly defined depth of closure.

3.3. Low-energy beach morphology

This section describes the typical beach profiles found for beaches in low-energy environments as well as the long-term development of low-energy beaches. An understanding of the different beach shapes helps to characterize what type of forcing is present on the PHSD. Long-term development gives hints about future development of morphology of the PHSD.

3.3.1. Common beach profiles

The general shape of low-energy beaches is similar to profiles found in laboratory experiments with constant wave forcing representative of low-energy environments on an initial slope of sediment. These laboratory results conclude that an equilibrium profile is reached with a subaqueous platform. Surface waves erode the initial slope, and the sediment is deposited on the platform. With equal forcing and no water level variations, this platform reaches the depth of closure, a depth where wave action becomes insufficient to mobilize sediment.

Typical features of low energy beaches are the presence of small aeolian dunes (Jackson et al., 2002), a narrow and steep foreshore, and more seaward a low-gradient subaqueous platform that may be vegetated (often referred to as ‘low-tide terrace’ or ‘platform’).

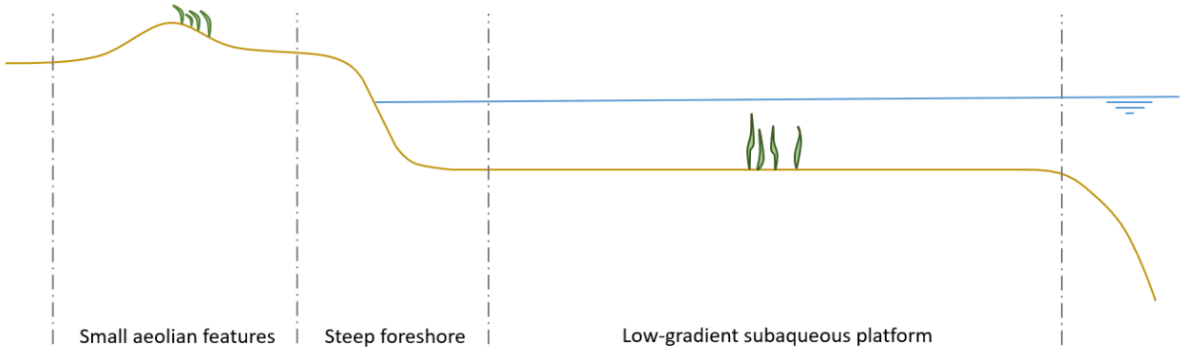

Figure 3.2: Typical cross-section of a low energy beach.

Low energy beaches exist under a wide range of circumstances that shape the beach profile. Multiple efforts were made to classify these low-energy beaches and describe typical profile shapes in morphotypes (Hegge et al., 1996) (Wright & Short, 1984). Similarities have been found between these studies by (Ton et al., 2021), that conclude that the least wave-exposed sites generally have the steepest and narrowest beach face and the strongest breaks between the swash zone and the

subaqueous platform. Furthermore, all models indicate wave climate and sediment characteristics to be the dominant drivers for different morphotypes to prevail.

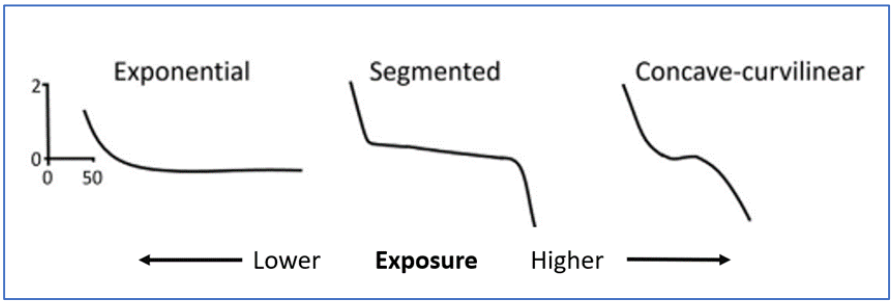

Figure 3.3: Morphotype model for low-energy beaches (Ton et al., 2021) *based on wave energy exposure. Less exposure leads to a more pronounced low-gradient platform while less exposure leads to a plane slope.*

3.3.2. Multi-decadal behavior

Multi-decadal behavior is essential for understanding low energy beach evolution as typical erosion and recovery timescales are much slower than those typical for open ocean coasts. Low-energy beaches are often found in estuaries or embayed environments where a wide range of settings is possible, influencing the long-term behavior. Based on the relative influence of those settings, a typology for decadal behavior has been distinguished, introducing four decadal behaviors: (1) 'prograding', (2) 'quasi-stable', (3) 'retreating' and (4) 'storm relict' (Fellowes et al., 2021).

Swell-exposed beaches, near the entrance to open ocean, are often quasi-stable and show recovery timescales comparable to that of open ocean beaches (smaller than three years). In contrast, beaches further from the entrance and less swell wave exposure show generally larger timescales (3-15 years) and will only be *quasi-stable* if storms are sufficiently infrequent. Prograding beaches are typically far from the entrance, where fluvial and tidal processes dominate and erosion events due to wind waves are less pronounced.

(Fellowes et al., 2021) found that low energy beaches recover (prograding & quasi-stable), partially recover between storms (retreating), or never recover (storm relict) depending on storm frequency and intensity, recovery potential, presence of sediment sources and sinks, and anthropogenic interventions.

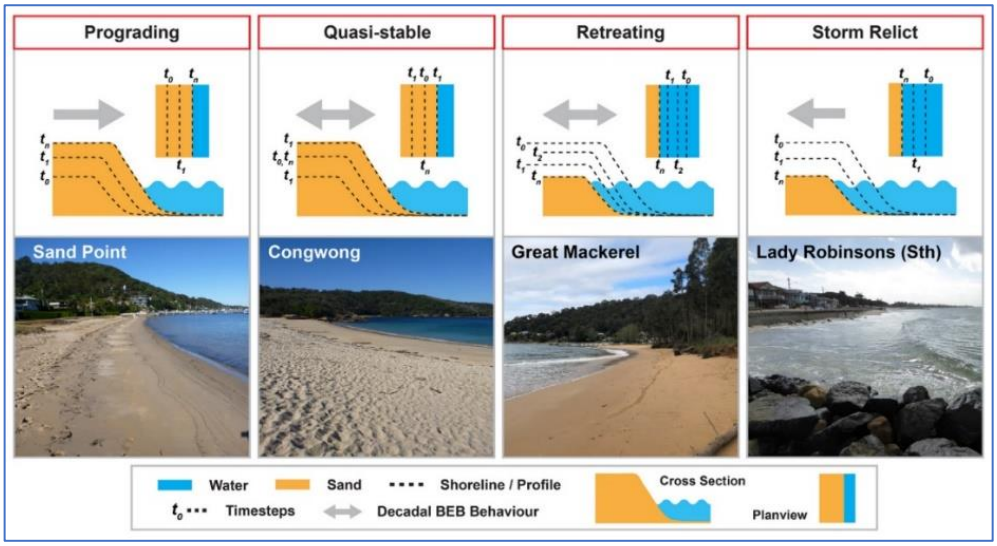

Figure 3.4: Typology of multi-decadal morphological behavior for low-energy beaches (Fellowes et al., 2021).

4. Morphology

Morphologic data-analyses reveals the behavior of the PHSD as a result of hydrodynamic and aeolian forcing. A morphologically stable coast is considered beneficial for longevity of the flood defense and for ecological value creation within the PHSD area.

The first section describes the methods used to analyze drone data. Later, trends in erosion and accretion are presented along the studied coastline alongside total volume losses of different regions on the PHSD. Afterwards, spit head growth and closure of the tidal opening is analysed. Lastly, the wind climate during the four-year period of PHSD service lifetime reveals intensity of forcing conditions, to check if changes in morphology are representative of future development.

4.1. Methods

This section elaborates on the methods used for the processing of drone data for analyses on morphological development and trends.

4.1.1. Volume calculation

The studied coastline is subdivided into different regions based on a height criterion. Areas above 1.85 m+NAP are considered to be part of the supra-tidal area; hydrodynamic forcing is hypothesized to have reduced influence on morphology as water levels infrequently rise above. The area between 1.85 m+NAP down to the spatial coverage of the elevation datasets is called the intertidal area, which is subdivided into three sections based on orientation of the shoreline.

- The NIOZ harbor section is characterized by a shoreline orientation of 40 degrees North.
- The Elongated spit section is to the Northeast of the NIOZ harbor section and has a general shoreline orientation of 50 degrees North.
- The Spit head section on the Northeast end of the studied coastline with a shoreline orientation that gradually rotates from 50 towards 0 degrees North.

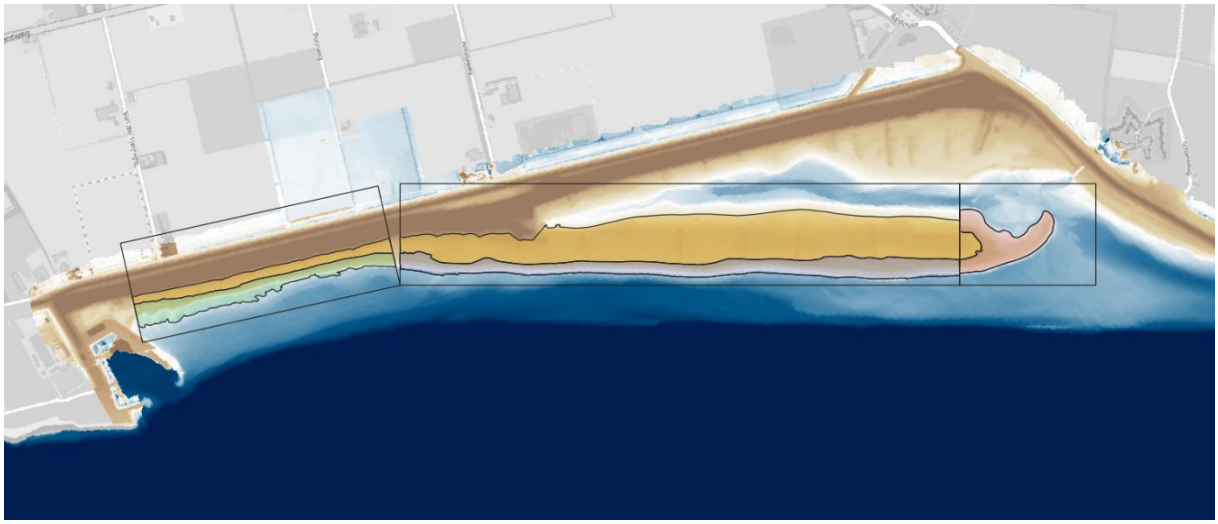

Figure 4.1: The different areas distinguished on the PHSD; the supra tidal section (yellow), the NIOZ harbor section (green), the elongated spit section (blue) and the spit head section (red).

Total volume changes of different sections are calculated. The procedure for calculating cumulative volume changes for the NIOZ harbor region and the Elongated spit region is as follows.

The outline of drone data coverage is extracted. If a dataset has significantly smaller spatial coverage than most of the other datasets, the dataset is removed from the analysis to extend the

spatial coverage (a trade-off is made between temporal and spatial resolution). The largest area covered by all the remaining datasets is extracted and determines the outer boundary for the analyses. This ensures that volume changes are the result of bed level changes only. The outer boundary is used to determine the extent of the raster layers containing spatial elevation. All datasets are subtracted from the base layer, which is the first drone measurement in 2019Q3. The mean height of the different regions is calculated and multiplied with the total area of that region to find volume change.

$$dV_i = (\Delta h_{i,mean} - \Delta h_{2019Q3,mean}) \cdot Area$$

Calculating volume changes for the spit head region requires a different approach. Because of growth of the spit head, a calculation of volume differences based on a largest common area approach would be limited to the bounds of the first measurement (Fall 2019) as the spit head is smallest at this point in time. This approach does not represent the total volume increase over time. The area used for volume change analyses is now based on a height criterion. The measured area that does not comply with the height criterion is eliminated from the analysis.

$$Area_{analyses} = Area_{measurement,i}(h > -0.2\ m + NAP)$$

The first measurement in Fall 2019 contains topographic and bathymetric data, this layer is used as the base layer to calculate cumulative volume changes. Volume changes are now calculated as the summed difference in height of a drone measurement and the first drone measurement.

$$dV_i = \sum(\Delta h_i - \Delta h_{2019Q3})$$

Be aware that the spatial boundary of the analyses is updated every time step in order to account for the gradual spit head growth.

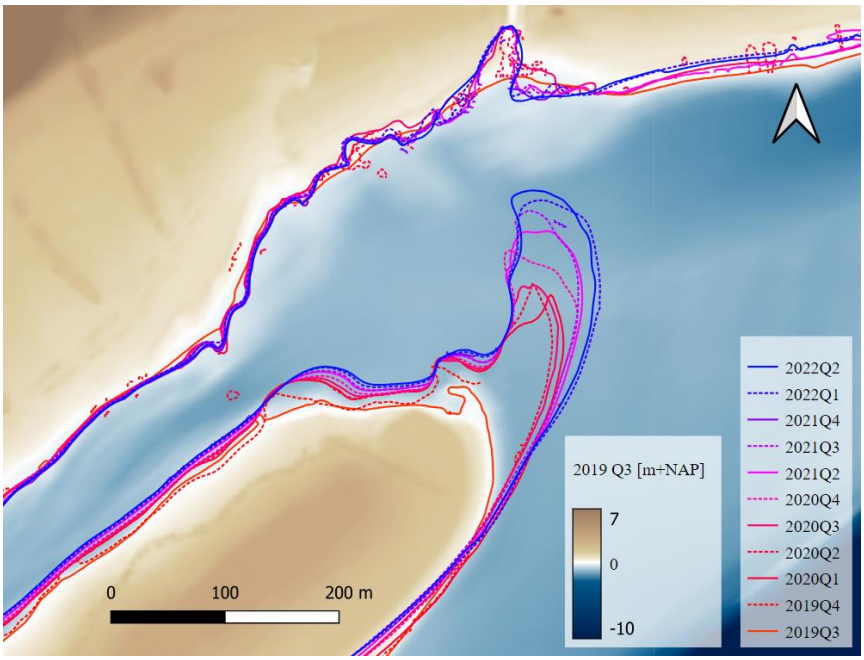

Figure 4.2: Outer boundaries of volume change analysis for the spit head section. The lines represent the -0.2 m+NAP contour lines for each drone measurement.

For cumulative erosion and deposition trends as a function of x-axis, the procedure above was followed but instead of calculating volumes per region, it is now calculated for a finer spatial grid. A grid with a cell width of ten meters is placed over the PHSD regions, seen in (Figure 4.3). This method obtains erosion and deposition on a ten-meter longshore resolution.

The data used for this analysis contains spatial grid of elevation data measured by a LiDAR drone performed by the contractor; Jan de Nul. Spatial resolution of the data is two by two meters and the interval between drone measurements is approximately 3 months.

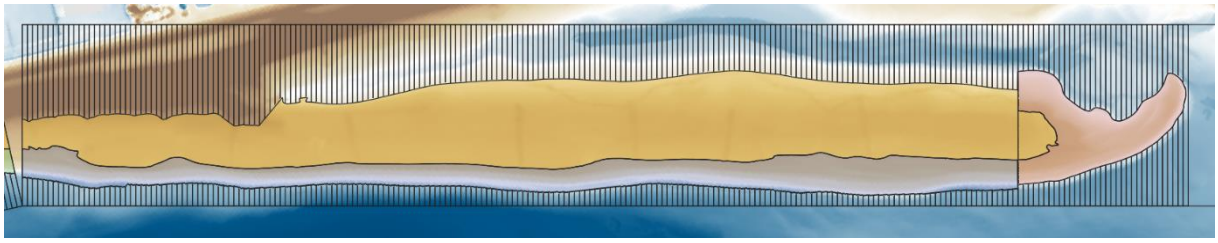

Figure 4.3: Grid, with 10-meter spacing, placed over the studied coastline to obtain cumulative erosion and deposition as a function of longshore position.

4.1.2. Profile extraction

Two transects are defined for analyses of development of the spit head and tidal opening of the lagune, seen in (Figure 4.6). Height profiles are extracted from spatial data containing topographic and bathymetric measurements. This type of measurement is performed once a year, resulting in three years of data for this analysis.

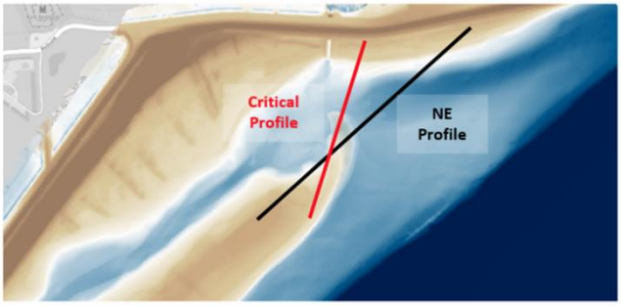

Figure 4.4: Defined profiles used in analyses for the development of the tidal opening.

4.2. Trends and volume changes

Volume changes during the full lifetime of the PHSD are presented in this section. The results indicate erosion, accretion, or quasi-stable behavior of the different regions. Calculation of volume changes is performed as described in (4.1).

4.2.1. Morphological trends of the intertidal zone

The spit head, elongated spit and harbor regions are sections within the intertidal zone where hydrodynamic forcing is assumed to be the most influential for the observed morphological changes. Cumulative volume changes of these regions are shown in (Figure 4.5).

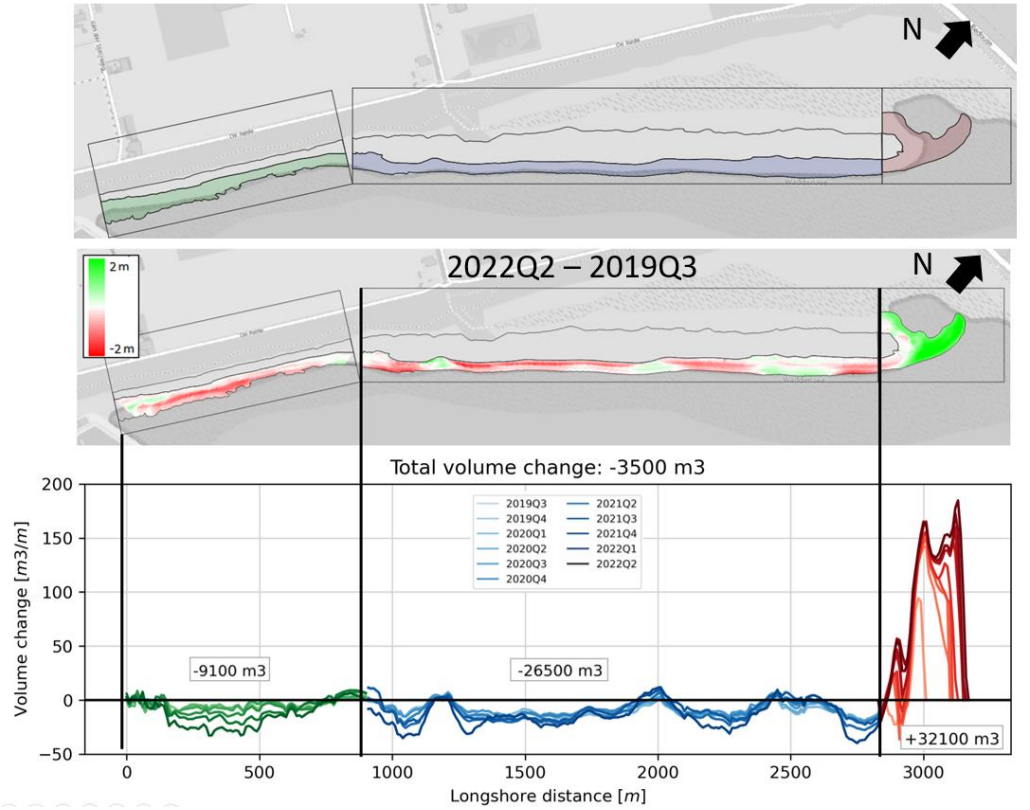

Figure 4.5: Upper panel) Different regions defined on the PSHD. Middle panel) Elevation differences between the last and the first drone measurement, with net erosion indicated in red and net deposition in green. Lower panel) Cumulative volume changes (with respect to 2019Q3) as a function of the longshore distance. Positive (negative) values indicate net volume loss (increase), and the colors indicate which area is considered in the analyses.

Deposition is seen as the spit head extends in NE-direction. This can be seen by volume increases to shift further longshore over time. The spit head has extended two-hundred meters Northward and has an average width of seventy meters. The biggest volume increase occurred in the first winter after construction (2019Q4 and 2020Q1), see (Figure 4.6). After this initial jump, the spit head continues to grow in volume at a consistent rate. The total volume increase reaches +32100 m^3 after three years of development.

The elongated spit faces erosion of the coastal profile. In total, the elongated spit has eroded -27.000 m^3. Two-thirds of this volume had already occurred within the first winter (2019-2020). This period coincides to the jump in volume increase of the spit head. After the initial jump in erosion the volume is relatively constant and little to no changes occur. In the winter of 2021-2022 a second jump in erosion occurs. Although overall erosion is found on the elongated spit, there are a few zones where

volume has increased. These zones coincide with local variations in the shoreline orientation. On these exact locations, the shoreline bends towards the North and later restores to the average orientation of the elongated spit.

The Harbor region experiences net volume losses. However, where the elongated spit and spit head showed initial jumps in morphological development, the Harbor region shows a more continuous trend; erosion steadily increases up to a total of -10.000 m^3 (2022Q2).

4.2.2. Total volume changes per region

Net volume changes indicate if erosion and accretion rates are accelerating, stable, or decelerating. Furthermore, the supra-tidal zone is considered within this analysis to assess morphological stability of the studied coastline more inclusively. Net volume changes of the regions, as defined in (4.1.1), are shown in (Figure 4.6).

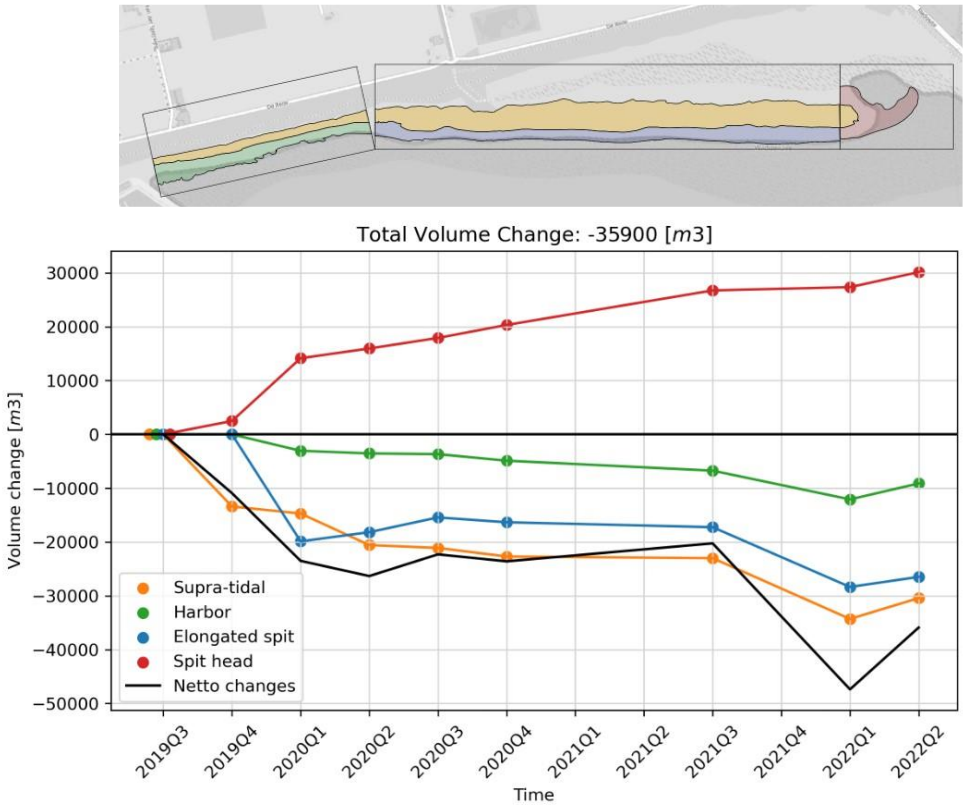

Figure 4.6: Upper panel) Different regions distinguished on the PHSD. Lower panel) Cumulative volume changes per region.

The volume of the spit head increases at a consistent rate. This increase is observed both in winter and summer, indicating net longshore transport towards the Northeast throughout the entire year.

In contrast, volume changes on the elongated spit are not consistent. During the first winter (2019Q4-2020Q1), volume decrease is significant while the volume on the spit head increases. Two-thirds of the total volume changes occur in the first winter (2019Q4-2020Q1) and the remaining erosion occurs in the third winter (2021Q3-2022Q1). The latter indicates erosion-events to be more episodic of nature. Directly after erosion events, slight rebuilding is seen by an increase of volume (2020Q1-2020Q3). Overall, this section looks to be storm-relict, as rebuilding does not restore eroded volumes.

The coastline of the NIOZ-harbor region shows less, but constant erosion over time. Summer and winter months all contribute to structural erosion in this section. Averaged over the full intertidal zone; a net erosion of 3500 m^3 has occurred. The volume decrease of this region results in gradual retreat of

the shoreline, see (Appendix A: Cross-shore profile development Transect 6), This is important as this section has a function as primary flood defense.

Volume changes of the supra-tidal region show substantial erosion throughout the full lifetime. Taking all intertidal regions and the supra-tidal region into account; total volume has decreased 36.000 m^3 on the PHSD within the studied area.

4.3. Spit head and tidal opening development

To analyze the development tidal opening of the lagoon after 3 years, two profiles have been defined along which elevation data is extracted, see (Figure 4.7). The first profile is called the 'NE Profile' and is chosen equal to the profile assessed in the model study. The second profile is called the 'Critical profile' as it is aligned with the narrowest part of the tidal inlet and the direction of the spit head extension. Bed elevation data from on-site measurements are extracted along the profiles and are shown in the lower two panels of (Figure 4.7). A comparison with model study for tidal inlet properties is shown in (Table 4.1).

The spit head extension and volume increase is significantly larger than predicted in model study (Witteveen+Bos, 2016)The tidal inlet width decreased by 200 meters in three years as a result of the extension of the spit head. Furthermore, the average depth has decreased 0.40 meters (from -0.9 m+NAP to -0.5 m+NAP). As a result, the conveyance area of the tidal opening has decreased 77% since construction.

Spit head growth rate is fairly consistent and does not decrease significantly over time, as described in (4.2). It is likely that within the upcoming years the conveyance area will have decreased to the point that the tidal lagoon will not be in open connection with the Wadden Sea during low-water.

The model study predicted spit head growth to be in Northeast direction, in line with the orientation of the elongated spit. In reality, the extension of the spit head has rotated more towards the absolute North, resulting in a more rapid decrease of the conveyance area. Furthermore, the extension length of the spit head was underestimated in the model study. Considering the constant nature of the spit head growth it is expected that the tidal opening will be closed within 2 to 3 years during water levels below MSL.

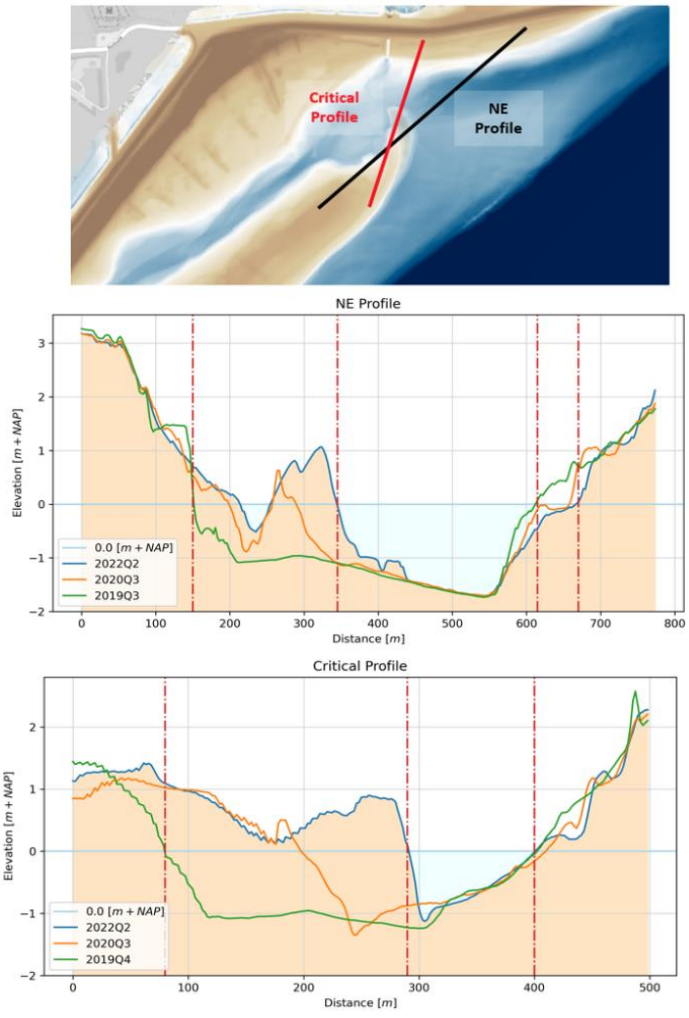

Figure 4.7: Upper panel) defined cross-sections for the analysis. Middle panel: NE profile development. Lower panel, Critical profile development.

Opening properties	**W+B Model Study** *NE profile*		**On-site data** *NE profile*		**On-site data** *Critical profile*	
	Initial	Three years	Initial	Three years	Initial	Three years
Spit head extension [m]	-	90	-	140	-	200
Average conveyance width [m]	550	450	465	325	320	120
Average conveyance depth [m+NAP]	-1.0	-0.8	-1.12	-1.05	-0.88	-0.53

Table 4.1: Summary of the morphological development of the tidal opening for the NE- and Critical profile.

4.4. Wind climate and storminess

In order to honestly assess the results found in this chapter, it is needed to evaluate the average wind climate over the four-years of service lifetime of the PHSD. The average wind climate based on a forty-year dataset is compared is compared to the wind climate during the four-years of PHSD service lifetime, see (Figure 4.8). Some differences are observed, such as a slight decrease in strong Easterly wind forcing (v_{wind} > 8.0 ms^{-1}) and a slight overrepresentation of South and South-Southwest winds. Aside from such minor, significant changes of the wind climate is not seen within (Figure 4.8). It can be concluded that the occurrence of different wind directions and strength of the winds have been fairly representative during the past four years.

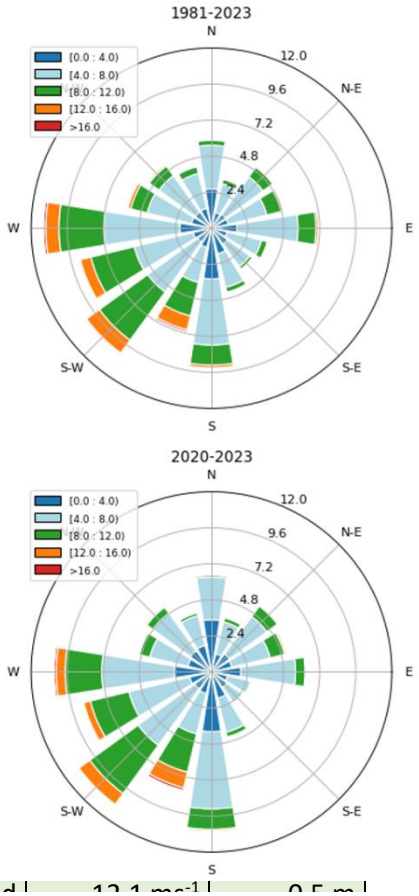

Figure 4.8: Wind climate in [ms^{-1}] based on KNMI data from measuring station de Kooij, near Den Helder.

Beaches in low-energy environments are characterized by 'storm-relict' behavior. Meaning storminess of the wind climate can have profound effects on morphology. Storminess of each year is listed in (

Direction	Southwest storms (v_{wind} > 10 ms^{-1})			Nort		
	Duration	Av. velocity	Av. set-up	Duratic		
2019-2020	39.0 d	12.1 ms^{-1}	0.3 m	3.3		
2020-2021	26.4 d	11.7 ms^{-1}	0.3 m	4.3		
2021-2022	24.0 d	11.6 ms^{-1}	0.3 m	2.0		
Average: 1981-2022	**32.6 d**	**11.8 ms^{-1}**	**0.3 m**	**5.2 d**	**11.1 ms^{-1}**	**-0.5 m**

Table 4.2). Years are considered to be from June to July the next year to group stormy winter periods. The table indicates that in the first year after construction (2019) Southwest storms were more prevalent, while Northeast storms were less prevalent compared to average conditions based on a forty-year dataset. This might explain the increased morphological development seen in the first year after construction. With 2019 being the stormiest year, this might explain increased erosion in the first year after construction, seen in (4.2).

Direction	Southwest storms (v_{wind} > 10 ms^{-1})			Northeast storms (v_{wind} > 10 ms^{-1})		
	Duration	Av. velocity	Av. set-up	Duration	Av. velocity	Av. set-up
2019-2020	39.0 d	12.1 ms^{-1}	0.3 m	3.3 d	10.4 ms^{-1}	-0.3 m

2020-2021	26.4 d	11.7 ms^{-1}	0.3 m	4.3 d	12.1 ms^{-1}	-0.5 m
2021-2022	24.0 d	11.6 ms^{-1}	0.3 m	2.0 d	11.5 ms^{-1}	-0.3 m
Average: 1981-2022	**32.6 d**	**11.8 ms^{-1}**	**0.3 m**	**5.2 d**	**11.1 ms^{-1}**	**-0.5 m**

Table 4.2: Storminess of the years during the lifetime of the PHSD. Years are represented including the full storm season (2019-2020 for instance; June 2019- July 2020).

5. Hydrodynamics

Hydrodynamic forcing, in the form of waves and currents, can initiate sediment transport when powerful enough. Over time, net sediment transport results in morphological development as was seen in (Morphology).

This chapter starts with an overview of hydrodynamic data measured locally at the PHSD. Wave and current forcing is characterized along the studied coastline. This overview characterizes the forcing climate and is later used in hindcasting forcing conditions in (Hindcasting forcing conditions). The next chapter describes the relation between wave forcing and set-up. This relation influences wave exposure at the steep shoreface and thus morphological development. The last chapter combines wave and current data to assess bed shear stresses on the elongated spit. Bed shear stresses indicate when sediment transport does and does not occur. Data from the SEDMEX campaign is used in this chapter.

5.1. Waves

This section is dedicated to exploring magnitude of wind wave heights along the studied coastline, showing spatial variability in wave exposure () and a derivation for the breaker criterion (5.1.2), both findings will be used in (Hindcasting forcing conditions) for hindcasting of wave conditions.

5.1.1. Wave exposure

Moments of increased morphological development align with moments of increased wind waves measured on the low-gradient platform (Appendix B: Cross-shore profile development (episodic)). As waves cause increased morphologic development, wave statistics during the SEDMEX campaign are shown in (Figure 5.1).

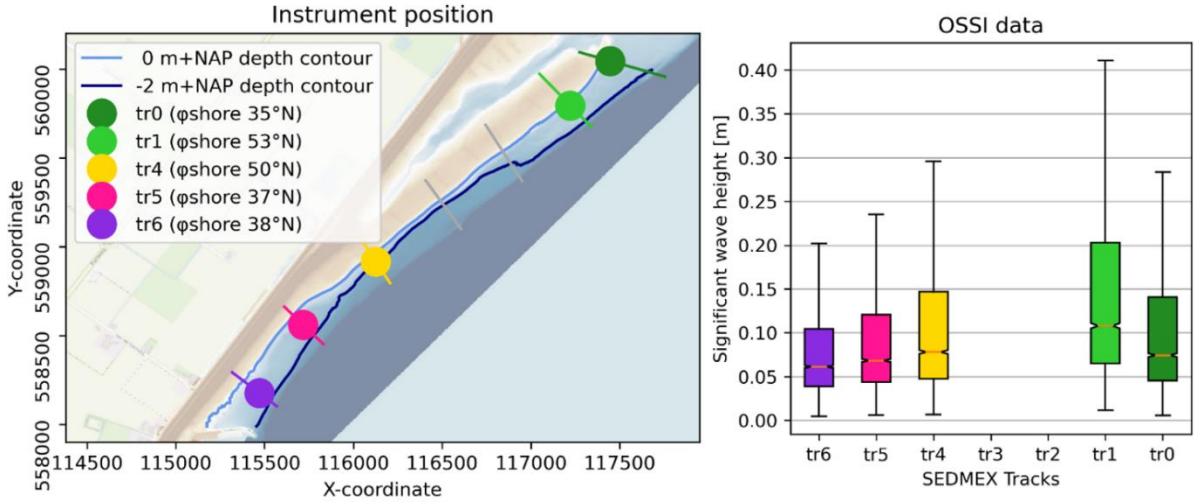

Figure 5.1: Left panel) Map-view of the PHSD and the placement of the OSSI wave measuring instruments. Right panel) Significant wave heights measured by OSSI's during the SEDMEX campaign using boxplots. The upper (lower) whisker indicates the 95th (5th) percentile significant wave heights, the upper (lower) edge of the box indicates 75th (25th) percentile wave heights and the orange middle bar indicates the median wave height.

Note that significant wave heights during the SEDMEX campaign are generally smallest near the NIOZ harbor and highest on the elongated spit. The boxplot shows both median and 95th percentile wave

height to be approximately twice as large near the elongated spit (transect 1) when compared to near the NIOZ harbor (transect 6). Considering wave-energy is quadratically related to wave height, wave-energy exposure at the elongated spit was approximately four times larger than near the NIOZ harbor. Furthermore, wave heights are significantly lower on the spit head (tr0) compared to the elongated spit (tr1). This is possibly due to the change in the orientation of the shoreline causing waves to refract and thus decrease in height.

5.1.2. Depth induced breaking

Depth-induced breaking occurs if waves travel in shallow water. The wave steepness increases to the point waves become unstable and break, resulting in turbulent motion and dissipation of wave energy. This is seen in a decrease in significant wave height. This phenomenon occurs normally near the steep shoreface as waves roll onto the beach. If water depth is low and waves are high, it is possible that depth-induced breaking occurs already on the low-gradient platform, thereby limiting wave heights near the steep shoreface. The latter is important as it limits the longshore transport potential.

An instance of depth-induced breaking is observed within the dataset of L2C10 (placed on the low-gradient platform on transect 1). This occurred on the night of 2 October when low water conditions coincided with a peak in offshore wave height (Appendix C: Summary of hydrodynamic conditions (SEDMEX)). At that moment, wave height on the low-gradient platform decreases suddenly while offshore wave heights peak, see (Figure 5.2).

From this event, the breaker criterion for wind waves on the low-gradient platform is derived data by dividing wave height measured at L2C10 by the local water depth. During depth-induced breaking the breaker criterion (H_s / d) was equal to $\gamma = 0.48$ [-]. In the remainder of this study, waves on the low-gradient platform are assumed to break on the low-gradient platform whenever this breaker criterion is met.

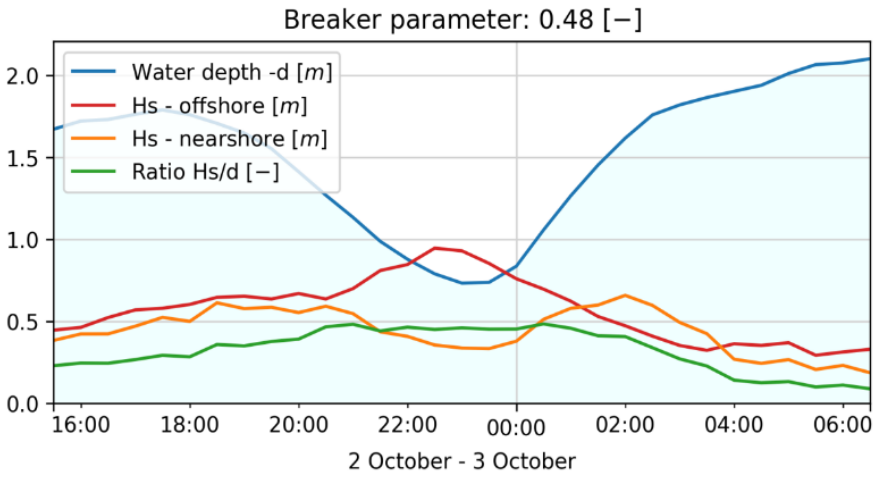

Figure 5.2: Breaker parameter estimation based on wave and water level measurements at L2C10.

5.2. Currents

Where waves often mobilize sediment by a stirring water motion, currents are able to transport mobilized sediment in the direction of the mean current. Currents on the low-gradient platform are a combination of tidal flow, wind-driven flow, and wave-driven flow. This chapter briefly describes current characteristics along the studied coastline using SEDMEX data derived from ADV's (SEDMEX campaign). Thereafter, the tidal component of the current is analysed by harmonic decomposition of the measured signal. Lastly, the influence of wind on tidal flow is explored using a conceptual model (Colosimo et al., 2020a) and wave-induced currents are approximated.

5.2.1. Alongshore variability

The current signal varies based on alongshore location on the PHSD. (Figure 5.3) shows the current signal represented in polar plots for different alongshore locations along the studied coastline. The ADV's are all placed at depths between -0.6 and -0.8 m+NAP on the steep shoreface. Currents on the low-gradient platform are typically aligned with local shoreline contours due to the steep shoreface acting as a hard boundary, resisting cross-shore flow. Current magnitudes are largest near the spit head and decrease towards the NIOZ harbor. On average, the current near the spit head are 40% stronger than near the NIOZ harbor. Furthermore, flood flow velocities are larger than ebb flow velocities, which indicates a flood dominant character of the tidal signal. The tidal asymmetry causes net flow over a tidal cycle to be in flood direction.

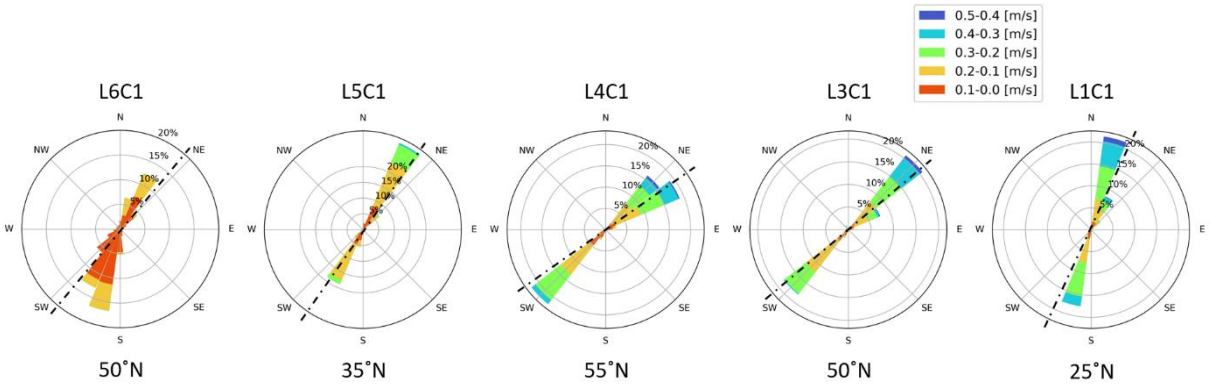

Figure 5.3 Polar plots of ADV's positioned on the shoreface between -0.6 and -0.8 m+NAP. From left to right placed near the NIOZ harbor along the coastline towards the spit head L1C1. Colors indicate flow speed and radial width indicates the percentage of time it occurs during the measurement campaign.

5.2.2. The effect of tides, wind, and waves on currents

Mean current measured locally on the PHSD is a combination of tidal-, wind- and wave-induced currents. This section describes all of the different contributors to mean current based on a decomposition of current signals, conceptual models, and first-order approximations. Although mean current is not simply a linear addition of the different currents, the order of magnitude does reveal relative importance of tide, wind, and waves.

Tidal flow

The tidal current on the low-gradient platform is analysed after a decomposition of the current signal at L2C10 based on the most important tidal constituents (M2, S2, O1, and M4), seen in (Figure 5.4). The procedure for decomposing the tidal signal is explained in (6.2). Current magnitudes are found to be as described in (Table 5.1).

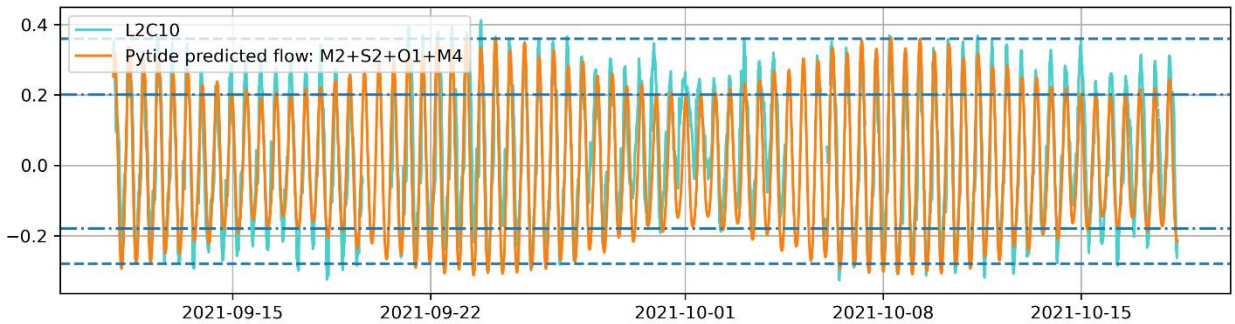

Figure 5.4: Measured longshore current [m/s] at L2C10 on the low-gradient platform and corresponding decomposed signal representing the tidal current.

	Spring tide [ms^{-1}]	Mean [ms^{-1}]	Neap tide [ms^{-1}]
Flood current	0.36	0.28	0.2
Ebb current	-0.28	-0.23	-0.18

Table 5.1: Spring, mean, and neap tidal current properties derived from decomposed signal with L2C10 data as input.

Flood flow velocity is on average larger than ebb-flow, as had been concluded in (5.2.1). Appendix (Appendix E: Cross-shore variation in currents) reveals tidal currents measured at the steep shoreface are approximately 40% decreased in magnitude compared to the low-gradient platform.

Wind-induced flow

The effect of wind, resulting in wind-driven flow, can reverse tidal currents, this is seen in (Appendix D: Effect of wind on tidal flow on the low-gradient platform). Wind speeds above 7 ms^{-1} directed in flood-direction have been seen to reverse tidal flow.

The effect of wind on tidal flow is determined analytically based on a conceptual model proposed by (Colosimo et al., 2020a). Winds aligned with flood flow direction enhance flood flow while diminishing ebb-flow. For wind speeds larger than 7 ms^{-1} ebb-flow is altered to flood flow. The opposite is also true, wind in ebb-flow direction enhances ebb-flow and reduces flood-flow. However, stronger winds are required to reverse flood flow. This is because flood flow is stronger than ebb flow due to the flood-dominant character of the tidal signal (5.2.1).

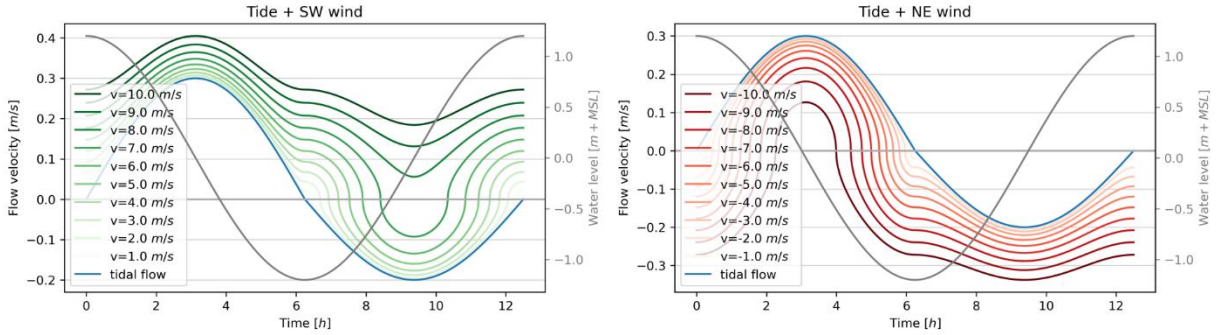

Figure 5.5: The effect on longshore tidal flow for Southwest wind (left) and Northeast wind (right). Tidal flow without wind influence indicated by the blue line. Green and red lines indicate combined wind and tidal flow under increasing wind speed, indicated by color intensity.

Wave-induced flow

Waves generate wave-induced currents when radiation stresses occur, observed in the surf zone near the steep shoreface. Indications of wave-induced currents are seen in data at L2C04 placed on the steep shoreface. Wave induced currents are approximated using the procedure in (6.2.3). Wave-induced currents are largest at the point of breaking and decrease linearly towards the waterline. The mean wave current in the surfzone is calculated for the mean angle of incidence of waves approaching the PHSD and increasing wave height. Significant wave heights between 0.2 [m] and 0.4 [m] can produce currents exceeding tidal currents near the shoreface. Wave-induced currents are therefore assumed to be important on the steep shoreface.

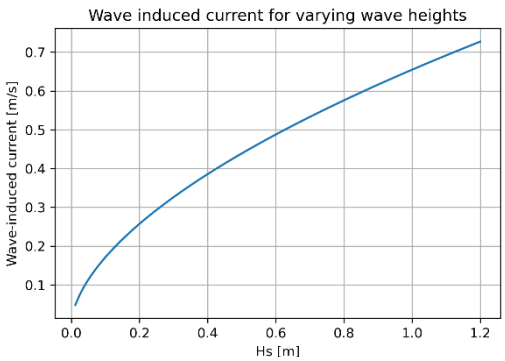

Figure 5.6: wave-induced currents based on average angle of incidence (20 degrees).

5.3. Interplay of waves and water levels

Wind causes the appearance of wind waves observed locally at the PHSD. Wind also causes set-up and set-down of the mean water level. Since both physical phenomena are related to wind forcing, the relationship between wave heights and water levels is examined for different wind direction and speed.

Water level set-up and wind wave height is shown for a range of different wind conditions in (Figure 5.7). Water level data is measured by a measuring station at Oudeschild, the dataset consists of water levels between January 2011 to June 2021. Water level set-up occurs generally for Southwest, West and Northwesterly winds. This phenomenon is most expressively observed during high wind speeds when water levels can reach up to 1.5-2.0 [m]. In contrast, set-down is observed for Easterly winds, the higher the wind speed the lower the water level.

Wave heights are measured by an offshore wave-buoy placed locally at the PHSD for a three-month period in the winter of 2021. The duration of the measurement is approximately three months. for a range of different forcing conditions. It is now seen that winds from the east do result in enlarged waves measured offshore of the PHSD but most likely is aligned with moments of lowered water levels. The opposite is true for South and South-Westerly winds, when increased wave heights coincide with water level set-up.

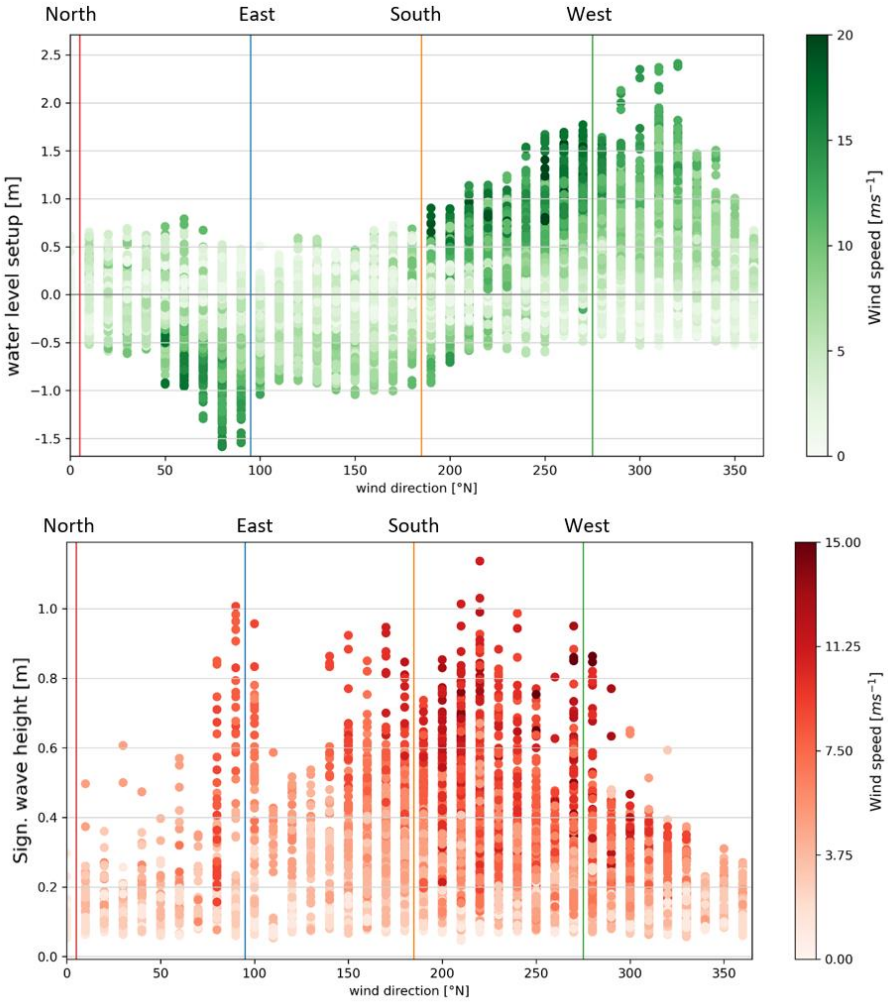

Figure 5.7: Upper panel) Water level variations plotted against wind direction and wind speed (color intensity). Lower panel) Wave heights measured offshore the PHSD plotted against wind direction and wind speed (color intensity).

5.4. Bed shear stresses

Bed shear is the controlling factor determining suspension and deposition of mud and sand in coastal environments. Bed shear stresses occur through current-, and wave-induced flow near the bed. The SEDMEX campaign is analysed to determine when bed shear stresses exceed critical values, initiating transport.

A time series of hydrodynamic properties and root mean squared bed shear stresses is analyzed in (5.4.2). Section (5.4.3) presents time series of calm and energetic forcing periods, the difference in maximum bed shear stresses indicate when transport occurs. The last section compares forcing conditions during in SEDMEX to an average annual forcing climate (5.5).

Bed shear stresses and sediment transport modes depend on sediment properties. These properties have been shown to vary spatially and temporally on the PHSD (Klein Obbink, 2021). Coarser sediment is found on the steep shoreface (d_{50} = 1.05 mm) than on the low-gradient platform (d_{50} = 0.56 mm). Furthermore, sediment compositions of the upper layer change as a result of calm or energetic conditions. Sediment properties influence bed shear stress magnitudes. For simplicity of the analysis, sediment diameters are assumed to be constant in time and space. The representative sediment distribution is presented in (Table 5.2). This table shows average values for sixteen sediment samples taken on the steep foreshore at -0.75 m+NAP along the studied coastline of the PHSD.

Sediment fraction	**Grain size (mm)**	**Critical bed shear stress**
D_{10}	0.272	0.18
D_{50}	0.557	0.28
D_{90}	1.939	1.22

Table 5.2: Overview of sediment properties used for bed shear calculations.

5.4.1. Bed shear stress timeseries

This section determines two moments of interest to be analysed in more detail. Both moments consist of three full tidal cycles (36-hour periods). Hydrodynamic conditions and bed shear stresses that occurred throughout the SEDMEX campaign is seen in (Appendix C: Summary of hydrodynamic conditions (SEDMEX)). The period around 26th of September (indicated with the green shaded area) corresponds to calm conditions and is elaborated in more detail in (5.4.2). The period around the 2nd of October is characterized by energetic conditions as wind speed picks up and wind waves are increased. A more detailed analysis of this period is seen in (5.4.3). This moment corresponds to increased morphological activity, seen in (Appendix B: Cross-shore profile development (episodic)).

5.4.2. Calm conditions

Calm conditions are analysed, an overview of hydrodynamic conditions is presented in figure (Figure 5.8).

Wind speeds during period 1 are low, which resulted in correspondingly low wave heights (Hs ≈ 0.10-0.20 m). Period 1 is characteristic for forcing conditions occurring most frequently on the PHSD. Two locations on the cross-shore profile are examined. ADV L2C4 is placed on the intertidal zone of the steep foreshore (at -0.5 m+NAP), this causes the sensor to emerge during low water which is seen in the left-hand plots by gaps in the data. The other location of interest is on the low-gradient platform where ADV L2C10 is placed. This sensor is placed at a depth of -1.4 m+NAP, therefore remaining fully submerged during the entire SEDMEX campaign.

The combination of low wave height and relatively high-water levels cause wave-orbital motion to be close to zero for the largest part of the tidal cycle. Only during low water conditions, it is seen that wave-orbital motion increases slightly and maximum bed shear peaks. Maximum bed shear barely

exceeds the critical shields stresses of D_{10} and D_{50} resulting in bed-load transport over a rippled bed. During times that maximum bed shear peaks, tidal flow is minimal as it occurs during flow reversal. Currents on the low tide terrace are weak (0.25 ms^{-1}) and do not result in mean bed shear stresses exceeding any critical value.

To conclude, Shields parameter values during low-energy conditions only barely exceed the threshold for motion and do not result in significant quantities of sediment transported. The low-gradient platform is not forced strong enough by either tidal currents or wave orbital motion to mobilize sediment. The low-gradient platform is therefore assumed to be inactive during low-energy conditions (H_s < 0.20 m). If transport occurs, the dominant transport mode would be wave-driven bed load transport over a rippled bed. Direction of net sediment transport is expected to be in the wave propagation direction as tidal flows are minimal during peaks in maximum shear stress

On the steep foreshore near L2C4 we see a similar result. Wave orbital motion peaks just before submergence when the ratio significant wave height over water level increases. Shields parameters however remain around the threshold of motion and sediment transport on the shoreface during low energetic conditions is limited. Nevertheless, it is interesting to see that tidal currents are significantly weaker on the shoreface area. This indicates sediment on the steep foreshore to be both mobilized and transported by wave-driven processes.

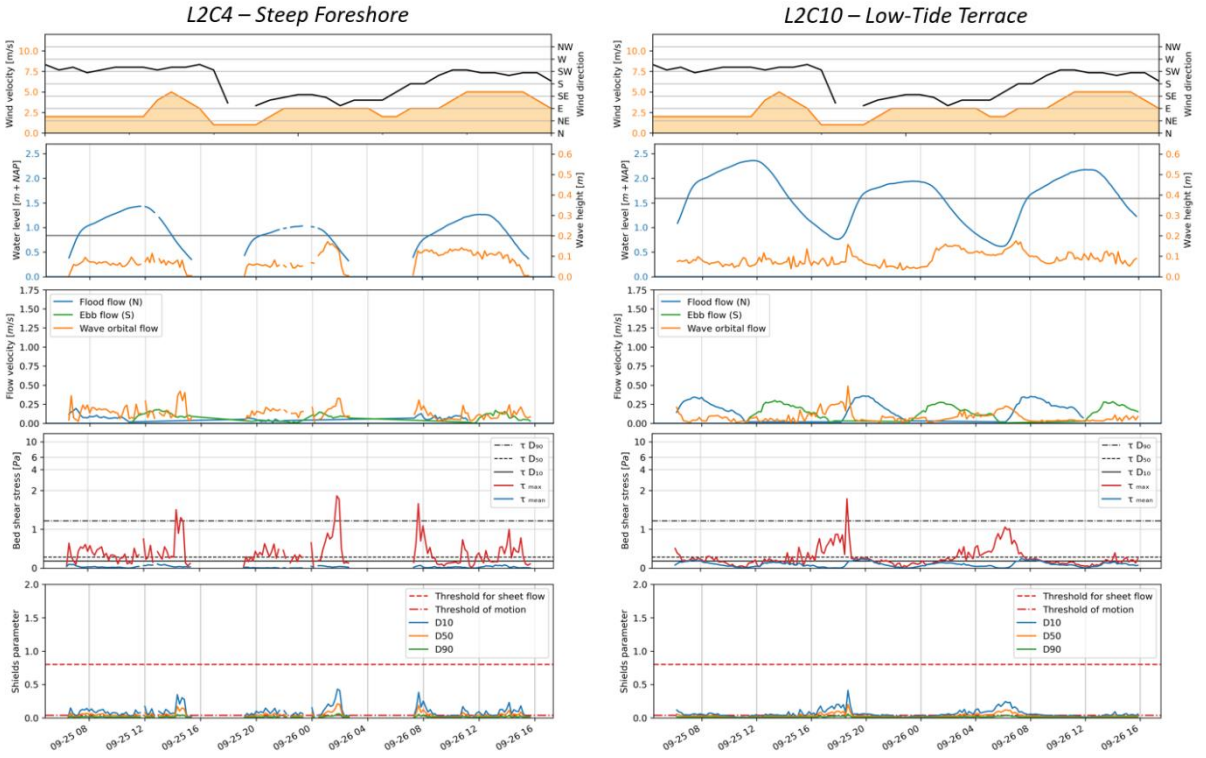

Figure 5.8: Data summary of a range of hydrodynamic conditions with figure on the left belonging to L2C4 (shoreface), and right L2C10 (low-gradient platform). The figures indicate wind forcing, water levels and wave height, mean currents and orbital flow, maximum bed shear and shields numbers (from top to bottom) for calm forcing conditions.

5.4.3. Energetic conditions

Energetic conditions are analysed, an overview of hydrodynamic conditions is presented in figure (Figure 5.9).

During period 2, wind velocity increases (from 8 to 11 ms^{-1}) as wind direction rotates from the West towards Southwest. This period represents typical moderate storm conditions from the dominant wind direction (Southwest). Nearshore significant wave heights gradually increase as the wind rotates

towards the South. Water depths are higher on average due to set-up in the Wadden Sea basin during Westerly winds.

At L2C10, the maximum bed shear stresses increase significantly resulting from larger wind waves. From the 30th of September 20:00 onward, wind blows from the SSW and increases towards 11 ms^{-1}. This results in larger wind waves (H_s > 0.4 m) resulting in maximum bed shear stresses above all critical stresses during the full tidal cycle. All sediment fractions are mobilized on the low-gradient platform. If the ratio of wave height and water level is high, maximum shear stresses increase and Shields parameters peak accordingly, implying sediment transport on the low-gradient platform to be wave-dominated.

strong winds blowing in flood direction influence mean flow on the low tide terrace, especially during ebb-flow. On the 30th of September 20:00, ebb flow is reversed, resulting in two tidal cycles (one day) of mean flow in flood direction. Furthermore, flood flow is lengthier but not significantly increased due to interaction with the wind. This corresponds to findings from (Colosimo et al., 2020a).

Concluding, Shields parameters are large but mostly remain mostly below 0.8, this indicates wave-dominated bed-load transport over a rippled bed. The direction of sediment transport is not known exactly through the effect of non-linear addition of wave and current motion. However, moments of highest shields parameters coincided with waves from the South and mean flow in flood direction (ebb-flow reversed to flood flow). Sediment transport is therefore assumed to be most plausible in the Northerly direction since asymmetrical orbital wave velocities and mean flow are both directed towards the North.

Similar findings are seen from the left-hand plots for L2C4 on the foreshore. Here bed shear stresses peak just before emergence and after submergence. Tidal flow velocities are minimal and was also seen in period 1 at L2C4. However, during the second tidal cycle when wind wave height is largest, the mean flood flow (blue line) suddenly increases towards 0.40 ms^{-1}. As tidal flows are much smaller in the vicinity of the foreshore, it indicates a longshore wave-driven current in flood direction. This wave-driven current remains in flood direction and facilitates sediment transport on the foreshore towards the North.

To conclude, net sediment transport on the foreshore is in the Northerly direction due to wave-driven longshore currents. Sheet flow limits are exceeded for the finer sand (D_{10}) within the sediment while the D_{50}, and D_{90} are most likely transported as bed-load.

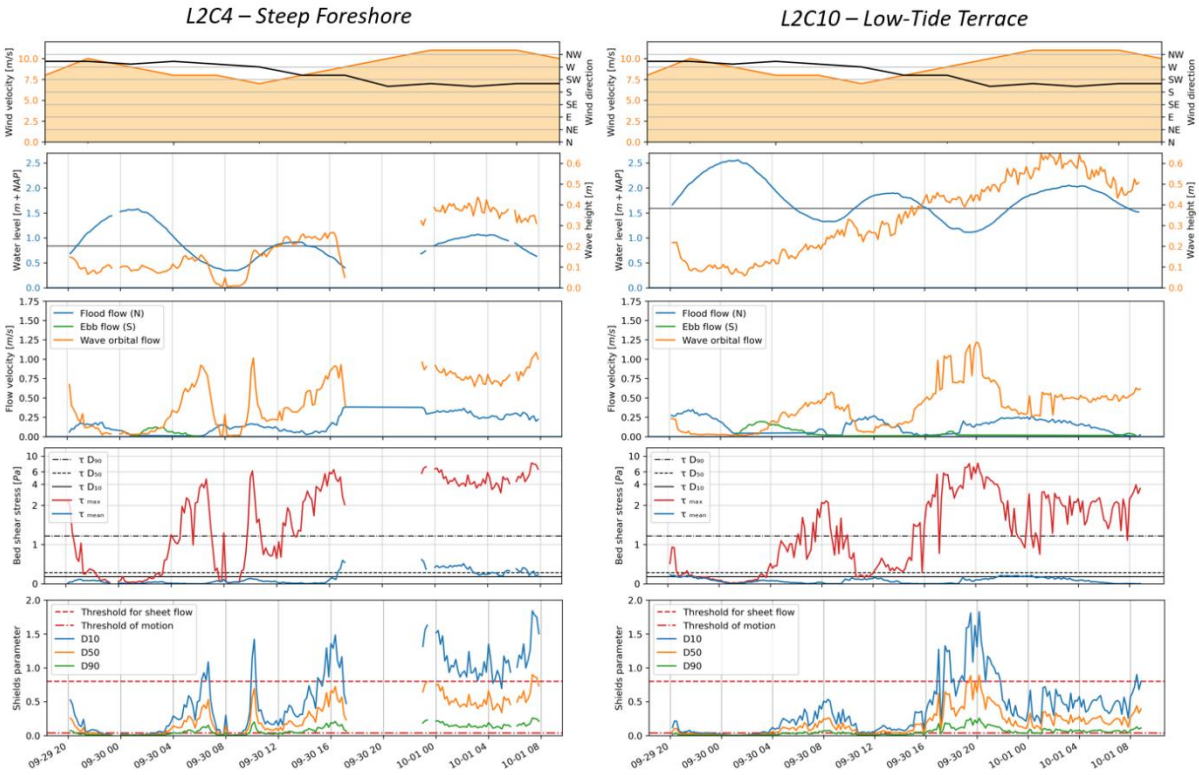

Figure 5.9: Data summary of a range of hydrodynamic conditions with figures on the left belonging to L2C4 (shoreface), and right L2C10 (low-gradient platform). The figures indicate wind forcing, water levels and wave height, mean currents and orbital flow, maximum bed shear and shields numbers (from top to bottom) for energetic forcing conditions.

5.5. Wind climate

Winds from the SW and S where well represented during SEDMEX forcing data. Moderate storm conditions prevailed from the SW, S and S between 28th of September and 4th of October. Storms from the S and SW sectors can however be more intense with hourly averaged wind speeds measured up to 20 ms-1. Such conditions did not prevail during SEDMEX but are deemed essential to morphological development.

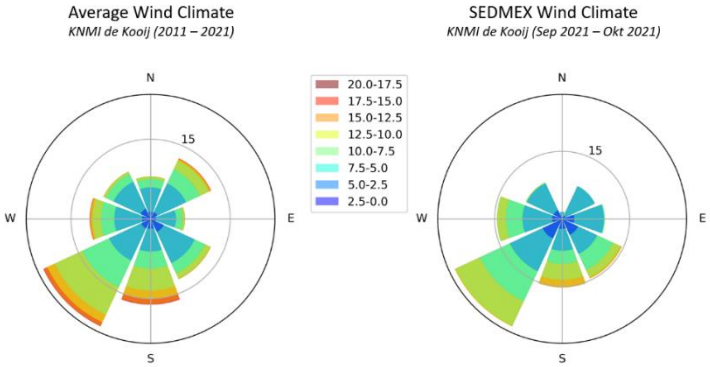

Figure 5.10: Left) Polar plot of wind speed (color), wind direction (angle) and frequency of occurrence (radial axis) for a ten-year KNMI wind dataset (2012-2022). Right) Polar plot, now for the SEDMEX campaign (September 2021 - October 2021).

Winds from the NE occurred although underrepresented during the SEDMEX campaign. Winds from the NE can be quite strong (10 to 15 ms^{-1}) based on the representative wind climate. Winds from this sector are believed to result in relatively large wind wave heights as fetch lengths are large (see Figure X). Note that fetch distances are dynamic resulting from tidal water level variations. Waves from the NE sector result in sediment transport towards the South (directed towards the NIOZ harbor).

6. Hindcasting forcing conditions

Morphological changes observed in (Morphology) are linked to hydrodynamic forcing observed in (Hydrodynamics) that result in net transport of sediment. Waves mobilize sediment, as was observed in (5.4), while mean currents determines the direction sediment transport. The limited timespan of wave and current data measurements complicates the comparison of longshore transport rates with observed morphological development. This is the reason a hindcast of waves and currents is performed based on readily available data.

$$U_{mean} = 0.60 \cdot (U_{TW}) + U_{wave}$$

6.1. Hindcasting waves

Longshore transport approximations require wave data. Limited span of wave data measurements complicate a comparison of longshore transport rates with observed morphological development. To address this issue, a simplified model approach is proposed based on empirical formulae for wave growth and analytical solutions for nearshore wave transformation. Since wave conditions are dependent on local wind conditions, wind data is used for approximation of offshore conditions. Furthermore, water level data is used to transform offshore conditions to nearshore conditions.

6.1.1. Offshore waves

Offshore wave conditions are approximated using an empirical formula (Kahma & Calkoen, 1992). This formula has been derived for young sea states in deep water conditions and approximates wave height for fetch-limited systems. Considering the limited fetch lengths within the Wadden Sea (5-20 km) and rapid response of wave conditions to local wind, it is believed that the assumptions underlying the Kahma and Kalkoen approximation are representative and applicable in this context.

$$H_{s,offshore} = a_1 \cdot \left(\frac{g}{{U_{10}}^2}\right)^{-0.55} \cdot F^{b_1}$$

Parameters	Physical meaning	Value and units	Data source
$H_{s,offshore}$	Offshore significant wave height	- [m]	-
a_1	Young sea state parameter	$2.88 \cdot 10^{-3}$ [-]	Kahma and Calkoen 1992
b_1	young sea state variable	0.45 [-]	Kahma and Calkoen 1992
g	gravitational acceleration	9.81 [ms^{-2}]	-
U_{10}	Wind speed ten meters above ground	Variable [ms^{-1}]	KNMI meteorological station 'de Kooij'
F	Fetch length	Variable [m]	RWS Vaklodingen 2019

Table 6.1: Table of properties required for the Kahma and Calkoen formula for fetch-limited wave growth in deep water.

The input parameters for the wave simulation model primarily consist of two variables: wind speed at a height of ten meters above ground level and fetch length. The wind speed data used in the model is obtained from continuous wind measurements conducted at the 'De Kooij' meteorological station by KNMI (Royal Netherlands Meteorological Institute). These measurements provide hourly averaged values of wind speed, allowing for an hourly representation of wind wave conditions.

To approximate fetch lengths within in the Wadden Sea basin, the -1 m+NAP depth contour is considered as the representative boundary for wave generation in this model (Figure 6.1). Although in reality fetch lengths may vary based on local water levels, this model assumes constant fetch lengths

for simplicity. Fetch lengths are determined for a range of wind directions. Measured wind direction from KNMI is used to select the appropriate fetch length, see (Figure 6.1). The wind direction data is averaged to ten-degrees.

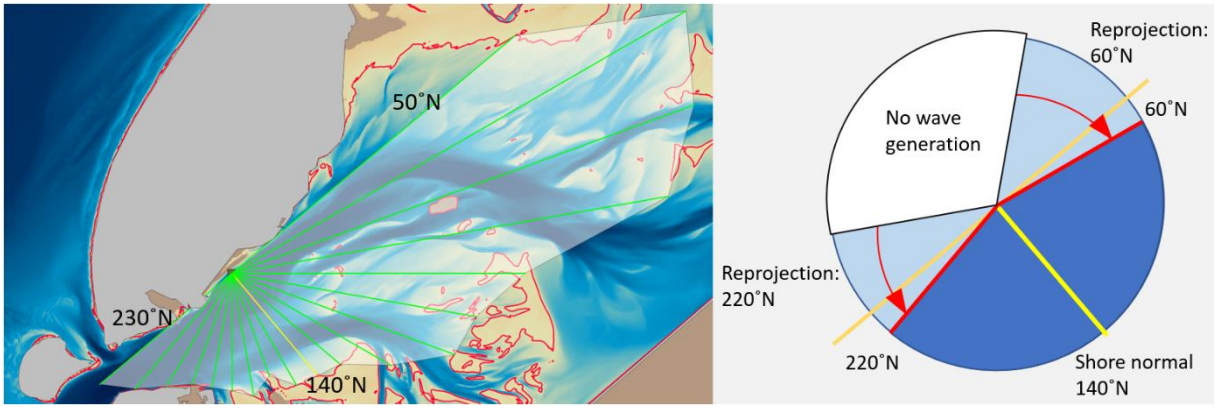

Figure 6.1: Left panel) Fetch lengths for different wind directions. Right panel) Excluded wind directions and reprojection of wind directions towards 220^{0}n and 60^{0}N.

By utilizing wind input parameters and incorporating averaged fetch lengths, the wave simulation model can generate hourly representations of wind wave conditions forcing the study area. However, it's important to note that the wave model has an inherent limitation. It does not take into account diffracted waves that travel around the NIOZ harbor and spit head. Despite this limitation, a significant amount of wave energy is observed resulting from wind conditions that are longshore or slightly offshore directed.

To address this, wind waves originating from wind directions between 270°N and 220°N are reprojected towards 220 °N. In addition, wind waves originating from wind directions between 10 °N and 60 °N are reprojected to 60 °N, see (Figure 6.1). Fetch lengths for all reprojected angles is set to three kilometers. This adjustment ensures that the model captures the effect of diffracted wind waves on the PHSD. Winds directions between 270°N and 10°N are considered 'offshore', which means they do not result in onshore traveling waves.

6.1.2. Nearshore waves

For longshore transport approximations, wave properties at the breakpoint is needed. To calculate nearshore wave conditions analytically, offshore wave height, wave angle of incidence and water levels on the low-gradient platform need to be known. Offshore wave height and angle of incidence is derived from offshore wave hindcast (6.1.1). Water levels are used from the Oudeschild measuring station is used, located four kilometers to the Northeast of the PHSD.

Wave conditions are determined at transect 1 as wave properties at this location will be used for longshore transport approximations. A cross-shore depth profile is used for calculating the dispersion location per horizontal step of 2.0 meters. The shallow water equations are calculated to account for shoaling, refraction, and depth induced breaking for waves propagating towards the steep foreshore. When the breaker criterion is met within the area of the steep-foreshore, wave conditions are saved at breaking point, and calculation stops. The output of this calculation is wave height and angle of incidence at breaking point.

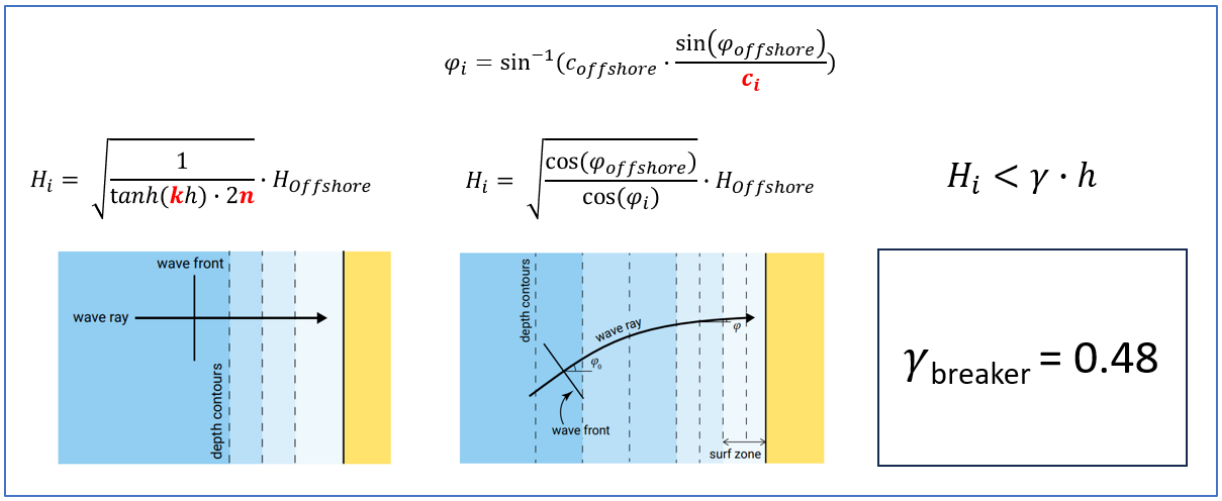

Figure 6.2: Calculation of nearshore wave conditions at the breaker. At first, the dispersion relation is solved iteratively. Later, calculation of shoaling, refraction and depth induced breaking is performed respectively. Whenever the breaker criterion is met, calculation stops wave conditions at the breaker are saved.

Validation of offshore and nearshore wave conditions is added in (Appendix F: Validation offshore wave simulation) and (Appendix H: Validation nearshore wave simulation).

6.2. Hindcasting currents

Longshore transport approximations explicitly accounting for currents require current data in the surfzone. Current data is not available and has to be hindcasted. Hindcasting of currents in the surfzone requires hindcasting of tidal, wind and wave-induced currents. Tidal currents are hindcasted through decomposing the tidal signal measured at L2C10 placed on transect 1 (6.2.1). The effect of wind-driven currents on tidal currents is incorporated by using a conceptual model proposed by (Colosimo et al., 2020a). The combined tidal- and wind-induced current is then decreased by 40%, as was seen in (Appendix E: Cross-shore variation in currents). Wave-induced currents are added linearly to nearshore transformed tidal- and wind-currents, yielding mean current at the steep shoreface. Note that this approach is a rough estimate as linear addition is not observed in reality.

6.2.1. Tidal currents

Using a harmonic analysis, the longshore tidal current is decomposed based on a set of tidal constituents (Table 6.2). Decomposition of the current signal measured at L2C10 is performed with the *pytides*-python package. The time series of currents fed to the decomposition is chosen carefully without significant data gaps and without high wind speeds. Gaps in the dataset are interpolated linearly.

Name	*Description*	*Period*
M2	*Principal lunar semidiurnal constituent*	*12.42 h*
S2	*Principal solar semidiurnal constituent*	*12.00 h*
O1	*Lunar diurnal constituent*	*25.82 h*
M4	*Shallow water overtides of principal lunar constituent*	*4.14 h*

Table 6.2: Tidal constituents used in the harmonic decomposition of the measured longshore flow at L2C10 using pytide.

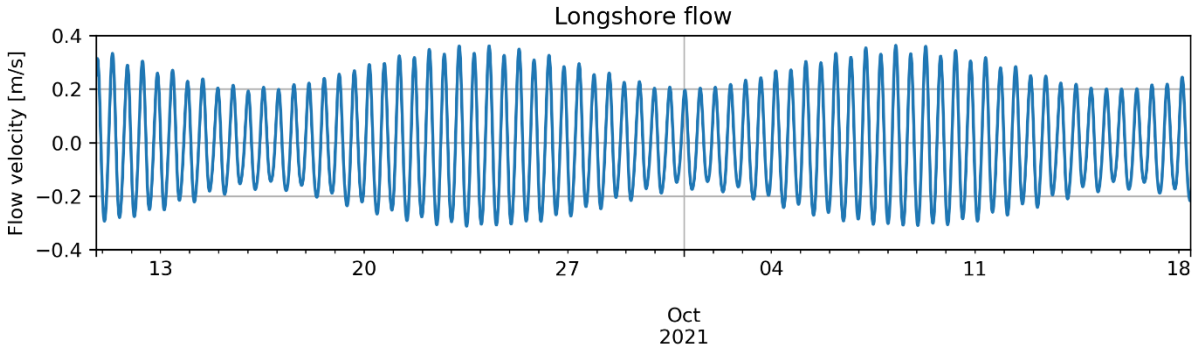

Figure 6.3: Longshore tidal current derived from current measurements at L2C10 using harmonic decomposition (pytide).

6.2.2. Wind-induced currents

Wind-induced currents are calculated using the conceptual model proposed by (Colosimo et al., 2020a), see the equation below The variables needed as input for this conceptual model are added in table (Table 6.3).

$$U_{TW} \cdot |U_{TW}| = U_T \cdot |U_T| + \frac{\rho_a c_D}{\rho_w c_{fw}} \cdot u_{10} \cdot |u_{10}|$$

Variable	Physical meaning	Value [units]
U_{TW}	Wind and tidal flow	To be calculated [m/s]
U_T	Tidal flow	Derived from decomposed tidal current (6.2.1) [m/s]
ρ_a	Air density	1.23 [kg/m^3]
c_D	Air drag coefficient	Formula (Wu, 1982)
ρ_w	Water density	1025 [kg/m^3]
c_{fw}	Bottom friction coefficient	$2.85 \cdot 10^{-3}$
u_{10}	Wind speed ten meters height above water	Derived from KNMI de Kooij wind station [m/s]

Table 6.3: Variables needed for the calculation of the wind and tidal current.

6.2.3. Wave induced current

Wave induced currents are calculated by using a simple analytical formula derived in (Bosboom & Stive, 2021, p370).

$$U_{wave} = \frac{5}{32} \cdot \pi \cdot \frac{H_b}{c_f} \cdot \mathrm{g} \cdot \frac{\sin \varphi_b}{c} \cdot \tan \alpha$$

Variable	Physical meaning	Value [units]
U_{wave}	Mean wave-induced current in the surfzone	To be calculated [m/s]
H_b	Significant wave height at breaker	Retrieved from wave hindcast (6.1) [m]
c_f	Friction coefficient	0.00285 [-]
φ_b	Wave angle of incidence at breaker	Retrieved from wave hindcast (6.1) [rad]
c	Wave propagation speed	Shallow water wave celerity [m/s]
α	Steepness of the shoreface	$6.25 \cdot 10^{-2}$ [m/m]

7. Longshore Transport Approximations

This chapter is dedicated to approximating longshore transport in order to assess the applicability of engineering formulae in their ability to describe morphological development in low-energy environments. Section (7.1) describes a schematization to compare longshore transport approximations to spit head growth studied in (4.3). Transport formulae include wave-only and wave-current longshore transport. Hindcasts of waves and currents derived as explained in (Hindcasting forcing conditions) are used as input for the formulae. The second section shows results from transport approximations and compares it to spit head growth.

7.1. Method

Schematization

Longshore transport is calculated for a representative cross-section on the elongated spit indicated by the red line (Figure 7.1), which is located in transect 1. Only the 'active profile' is considered in this analysis, which consists of the surf zone indicated by the red shaded area. The spit head is hypothesized to be a proxy for net longshore transport quantities and is used for comparison.

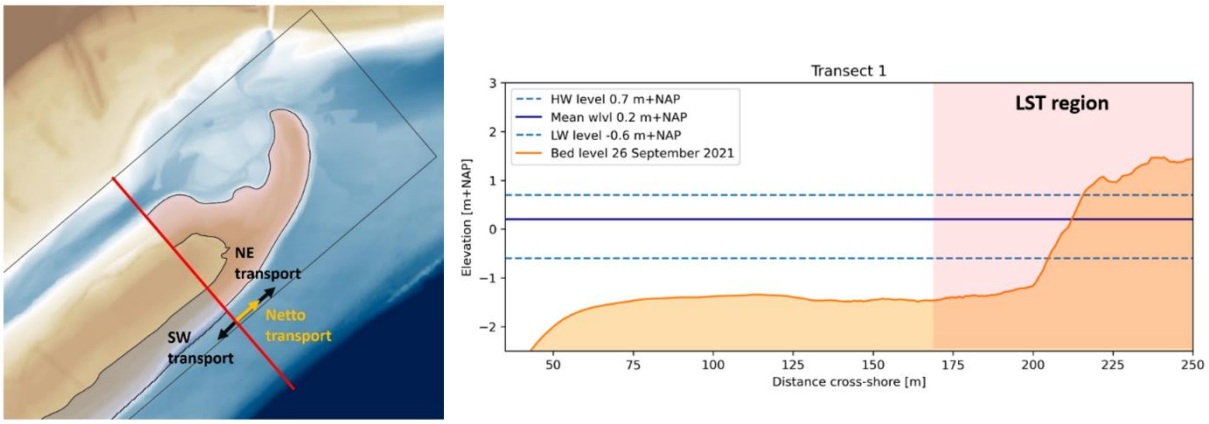

Figure 7.1: Schematization used for longshore transport rate calculations. Left, top view of the representative cross-section of the Elongated Spit. Right, indication of the longshore transport zone.

Longshore transport formulae

A brief description of the different bulk transport formula is provided along. The transport formula has wave simulation data at wave breaking as input.

Ingmar and Bagnold version of the CERC-formula (1963)

$$S = \frac{K}{16(s-1)(1-p)} \cdot \sqrt{\frac{g}{\gamma}} \cdot \sin(2\varphi_b) \cdot {H_b}^{2.5}$$

The formula above is the Inmar and Bagnold (1963) version of the CERC bulk longshore transport formula. Only wave-generated longshore current is considered (tidal and wind-driven currents are excluded). If longshore current is exclusively driven by waves, it is assumed both sediment concentration and longshore current to be related to wave energy and wave angle of incidence. Wave properties are used at the point of breaking, which in this case would be on the shoreface. Longshore transport is assumed equal to the power of 2.5. This is interpreted as a sediment concentration equal to the wave power E_b (hence H^2) and the transport velocity equal to u ($H^{0.5}$). The CERC formula does

not explicitly take into account wave period, bottom slope, and sediment properties. This formula has been derived for open coast systems.

Kamphuis formula (1991)

$$S = \frac{2.27}{(s-1)(1-p)} {H_b}^2 \cdot {T_p}^{1.5} \cdot (\tan(\alpha_b))^{0.75} \cdot D^{-0.25} \cdot (\sin(2 \cdot \varphi_b))^{0.6}$$

The formula above is the Kamphuis (1991) longshore transport formula. This formula explicitly accounts for grain size diameter, beach slope and wave period. However, relations for the grain size proportionality and beach slope on the sediment transport rate are weak. It should be considered that parameters within this formula are most-often interrelated. This relates to (α_b and D) as well as to (H_s, T_p, and ϕ_b). The explicit inclusion of wave and grain size parameters is hypothesized to make the formula better usable for sandy beaches in low-energy environments where such parameters are not interrelated. (Van Rijn, 2014) found the Kamphuis formula to significantly overpredict longshore sediment rates for calm conditions while underestimating transport rates during storm conditions.

Van Rijn formula (2014)

$$Q_{t,mass} = 0.00018 \cdot K_{swell} \cdot \rho_s \cdot g^{0.5} (\tan(\alpha_b))^{0.4} \cdot {D_{50}}^{-0.6} \cdot (H_b)^{3.1} \cdot \sin(2\varphi_b)$$

The formula above represents the (Van Rijn, 2014) longshore transport formula. Strong relationship between wave height at breaker and longshore transport is indicated by the wave height to the power 3.1. Also, a stronger relationship between D_{50} sediment grain size is in this formula. The formula can be rewritten to explicitly account for tidal and wind induced longshore current velocities possibly influencing sediment transport magnitude and overall direction. The latter is not done within this research. The formula was tested on a wide variety of sediment grain sizes and forcing conditions (wind- and swell waves).

Van Rijn + current formula (2014)

$$Q_{t,mass} = 0.00018 \cdot K_{swell} \cdot \rho_s \cdot g^{0.5} (\tan(\alpha_b))^{0.4} \cdot {D_{50}}^{-0.6} \cdot (H_b)^{2.6} \cdot U_{mean}$$

The formula above represents the (Van Rijn, 2014) longshore transport formula that explicitly accounts for mean current in the surfzone which is a combination of tidal, wind and wave-induced currents as calculated in (6.2).

7.2. Longshore transport compared to spit head growth

Transport rates are calculated for the 3.5 years since construction with the CERC, Kamphuis and CROS formulae. The cumulative longshore transport is presented in (Figure 7.2).

Firstly, all formulae predict net sediment transport to be in Northeastward direction (towards the spit head), which is in accordance with findings from (Morphology). Transport magnitudes differ significantly, up to an order of magnitude between CERC and van Rijn formulae. Nevertheless, the relative transport, seen in figure (Figure 7.2) lower panel, reveals signature of all four formulae are similar. This indicates two important findings. Firstly, all formulae have similar behavior. This was expected considering the main input for all formulae was wave height and wave angle of incidence. Secondly, the 'van Rijn+current' formula shows similar output as the traditional wave-only 'van Rijn' formula. This indicates that wave-induced currents in the surfzone are dominant with respect to tidal and wind-induced currents. The 'van Rijn+current' formula gives a slightly larger net Northeastward transport of sediment. This is also likely as the tidal signal is flood-dominant and the dominant wind direction is Southwest, imposing stronger currents in Northeastward direction.

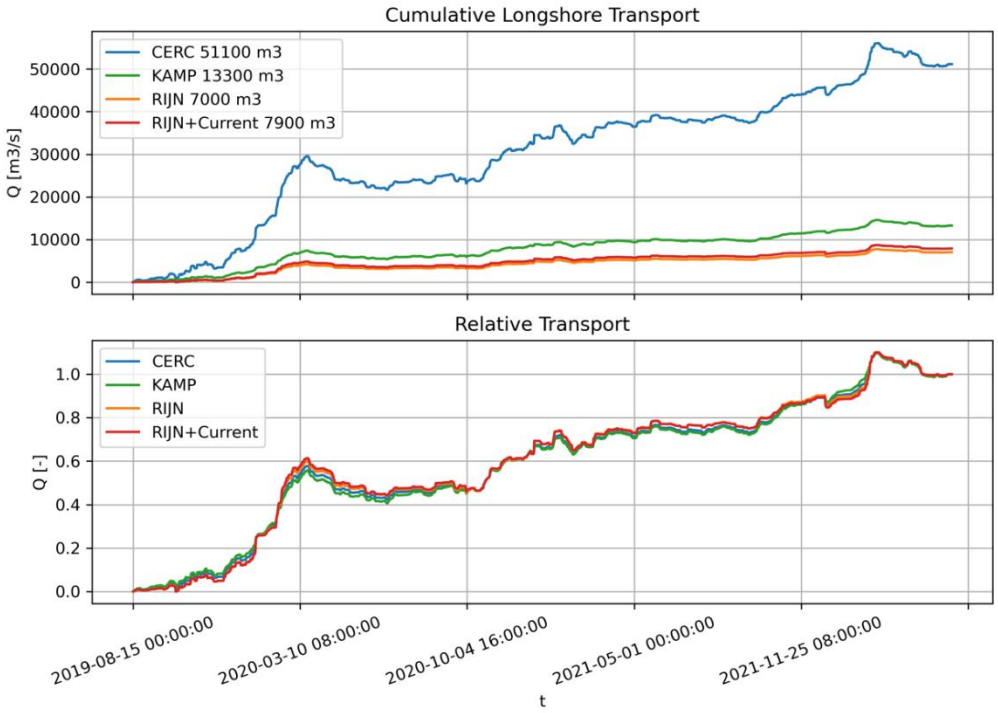

Figure 7.2: Upper panel) Cumulative bulk longshore transport calculated with 'CERC', 'Kamphuis', 'Van Rijn' and 'Van Rijn+current' sediment transport formulae. Lower panel) Relative sediment transport shown in the lower panel to highlight the similar signature of the four different transport formulae.

Longshore sediment transport is compared to spit head growth, which serves as a proxy for net longshore transport. *Cumulative transport calculated by CERC (total 51.000 m^3) results in the best approximation regarding total spit head growth (32.000 m^3).*

LST rates from wave-only transport formula are now aggregated for periods in between drone measurements and can be compared to spit head growth. Moments of increased spit head growth do coincide with moments of increased Northeast longshore transport. However, while volume increase of the spit head is consistent throughout the 3.5 years, predicted longshore transport shows periods of net Southward sediment transport.

Aggregated longshore transport rates are correlated to changes in spit head volume. All formula LST formulae have similar correlation values, see Table 7.1. Correlation for the CERC formula with spit head volume changes is presented in the scatterplot (Figure 7.3).

	Pearson R-value (Correlation coefficient)	p-value (significance of correlation)
CERC	0.85	0.00
Kamphuis	0.81	0.00
Van Rijn	0.77	0.01
Van Rijn+current	0.77	0.01

Table 7.1: Upper panel) Cumulative bulk longshore transport calculated with 'CERC', 'Kamphuis', 'Van Rijn' and 'Van Rijn+current' sediment transport formulae. Lower panel) Relative sediment transport shown in the lower panel to highlight the similar signature of the four different transport formulae.

There is one outlier present in the scatterplot seen in the top right corner (indicated by the orange dot color). This datapoint corresponds to the excessive spit head growth observed in the first winter after construction (2019Q4-2020Q1). The check if the correlation still holds without this datapoint, the outlier in the top-right corner is omitted. With omittance of the outlier, the correlation for CERC is still meaningful (R-value = 0.45, p-value = 0.26), although weakened from a strong correlation to a medium-weak correlation. This means that the CERC formula can represent trends in longshore transport at the PHSD. Magnitudes are however mostly under- or overestimated, therefore, calibration to specific low-energy conditions is necessary.

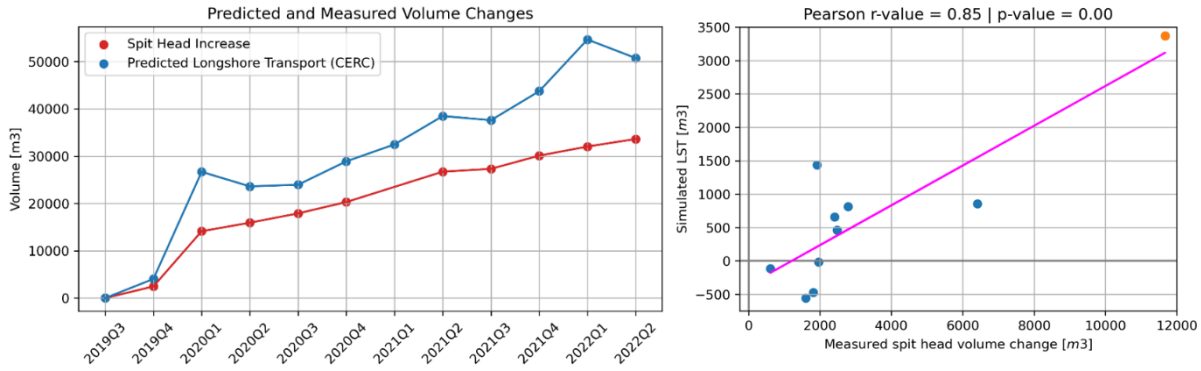

Figure 7.3: Left, measured cumulative spit head growth, and predicted LST using the van Rijn formula. Right, scatterplot of measured and predicted cumulative transport, the magenta line indicates the correlation of the two variables and the orange dot is considered an outlier, omitted for the analysis.

7.3. Morphological climate 2019-2022

The morphological climate is defined as the set of conditions which contribute most to the morphological development, in other words, to longshore transport. The morphological climate is schematized as the frequency of occurrence (1) of each forcing condition (wind velocity and wind direction) multiplied by the average longshore transport potential (2) of that forcing condition, calculated with CERC. The result is the average contribution of each forcing conditions to longshore transport (3). The three quantities (1, 2, and 3) described above are added in (Figure 7.4).

The frequency of forcing conditions reveals that South and Southwest winds are the most prevalent and occur with fastest wind speed (maximum wind speeds up to 22 ms^{-1}). Wind from all other directions is weaker but strong winds do occasionally occur.

It is observed that the potential transport increases as wind velocity increases for forcing from the South and Southwest. However, a different trend is found for forcing from the East and Northeast winds. With increasing wind velocity, the potential transport does not increase. In fact, above wind velocities of 8 ms-1, the potential transport decreases. This suggests that nearshore wave height decreases as wind velocity increases for Easterly winds.

The right panel, indicating the average contribution of each forcing conditions to morphological development, shows Southwest wind between 6 and 15 ms^{-1} contribute significantly to morphological development at the PHSD. Furthermore, Northeast winds show a hotspot of significant forcing conditions between 2 to 10 ms^{-1}. True storm conditions (v_{wind} > 10 ms^{-1}) from the easterly sectors do not influence morphological development.

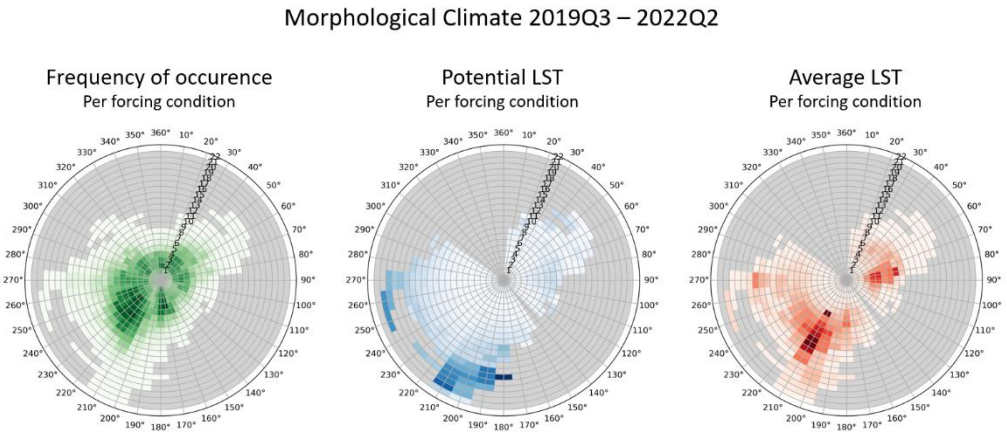

Figure 7.4: Left panel) Polar plot indicating frequency of occurrence of different wind forcing conditions. Middle panel) Polar plot showing potential transport per wind forcing conditions best on the CERC formula with 3.5 years of wave hindcasts used as input. Right panel) Average contribution of each wind forcing conditions to total longshore transport. Intensity of colors indicates the frequency, longshore transport potential and average contribution to total longshore transport.

As was observed in (5.3) the interplay of wave conditions and water level set-up and set-down shows systematic combinations. Strong Southwest and West winds cause increased wave heights to coincide with water level set-up, while strong Northeast winds cause increased wave height to coincide with water level set-down. Set-down can cause waves to break on the low-gradient platform due to the stringent breaker criterion that was derived in (5.1.2). As a result, true storm conditions from easterly sectors do not reach the PHSD steep shoreface. This is seen in a scatterplot of hindcasted offshore and nearshore wave conditions for the 3.5 years of service lifetime of the PHSD (Figure 7.5). Hindcasts of waves are performed as stated in (6.1) and thus include the effect of depth-induced breaking due to measured water levels at Oudeschild.

Offshore wave heights for easterly wind forcing can increase up to 1.6 [m]. However, depth-induced breaking limits these waves to 0.4 to 0.0 [m], most-likely because of depth-induced breaking on the low-gradient platform. Southwest waves also face a decrease from offshore to nearshore, but this is more likely the result of refraction than depth-induced breaking.

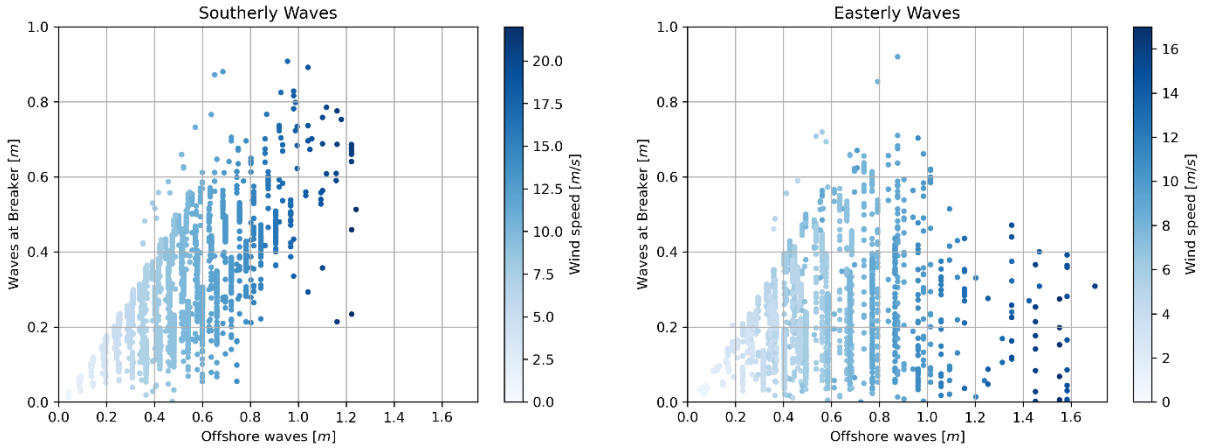

Figure 7.5: Left) Scatterplot of offshore and nearshore wave height for Southerly waves (resulting in net Northeastward transport). Right) Scatterplot of offshore and nearshore wave height for Southerly waves (resulting in net Southwestward transport). Wave conditions derived from 3.5 years of wave hindcasting as elaborated in (6.1).

8. Discussion

This chapter puts results presented in chapter 4, 5, 6, and 7 into perspective. Starting with a critical note on results obtained in this research. It does so by elaborating on the limitations of hindcasting forcing conditions (Hindcasting forcing conditions) and using engineering formulae to approximate longshore transport (7.2). Furthermore, it discusses the validity of using spit head growth as a proxy for net longshore transport.

The second section focusses on reflecting on a model study assessing the morphological stability of the PHSD (Witteveen+Bos, 2016). Some key assumptions made during this study are highlighted and reflected on with knowledge obtained within this research.

Lastly, the findings from this study are related to the findings of a study describing longshore transport on low-energy beaches by (Ton et al., 2023).

8.1. Review on research results

8.1.1. Applicability of transport formulae on low-energy beaches

Longshore transport formulae are calibrated to a wide range of beaches. These beaches include different forcing climates and different sediment grain sizes.

However, the CERC-, Kamphuis and Van Rijn formulae are all calibrated to datasets collected on ‘natural beaches’. Natural beaches generally have interdependency within different parameters, such as beach slope and grain size diameter, wave energy and wave height. This interdependency is also hidden within the sediment transport formulae, by being calibrated to those beaches.

In contrast, the PHSD is an artificially placed ‘unnatural’ beach. Interdependencies as described previously are therefore less self-evident. It is hypothesized that (uncalibrated) engineering formulae for longshore transport are less applicable asses longshore transports in low-energy systems. This could be seen by the large deviation between longshore transport approximation (using CERC, Kamphuis and van Rijn formulae) and morphological development of the spit head. It should be considered that a critical note is also added on using the spit head growth as a proxy for hydrodynamic sediment transport (8.1.3).

8.1.2. Accuracy of hindcasting

Wave forcing hindcasting

Longshore transport rates are approximated using simulated nearshore wave conditions as input. These simulated wave conditions are calculated using the Kahma and Calkoen wave growth formula for young sea states in deep waters (Kahma & Calkoen, 1992). Hourly averaged wind velocity and direction are the input parameters.

Offshore wind directions were reprojected to include wave energy from directional spreading of the wind wave signal and diffracted swell waves. The simplified wave model reprojects wind directions beyond 220 and 60 degrees North to the closest onshore direction. However, to accurately represent directional spreading of wind waves, a more fundamental approach is needed. Making a distinction in the degree of wave energy penetration based on offshore angle of incidence.

In addition, the simplified wave model does not account for swell waves. A study is needed on when swell waves occur locally at the PHSD and what the exposure to swell waves is of different regions along the studied coastline. The wave simulation model now accounts for them in a rather trivial manner by simulating wind waves.

Current forcing hindcasting

Current hindcasting was performed by hindcasting the tidal current, wind-effects on tidal currents and wave-induced currents in the surfzone. Currents are not a linear addition of the different current contributors, accurately assessing the nearshore currents can be a research project by itself.

For accurately hindcasting tidal currents, a larger dataset on longshore currents is preferably used. The harmonic decomposition (6.2.1) considers four of the five most prominent tidal components (M2, S2, O1, M4). The N2-tidal component could not be decomposed successfully. It is hypothesized that this is the result of the duration of the current dataset that is fed into the decomposition algorithm. A better decomposition of the tidal signal requires a non-interrupted (no gaps) and lengthy timeseries of current conditions during low-wind conditions (summer period).

Wind-effects on tidal flow have been approximated using the conceptual model proposed by (Colosimo et al., 2020a). Variables needed for input of this model have been set to commonly found values (drag coefficients, and water and air densities). Accurate usage of the model requires site specific values for these variables and calibration to actual measurements.

Lastly, wave induced currents are derived using a simple analytical formula with hindcasted waves as input. Approximated wave driven currents should be compared to on-site measurements to derive the validity.

8.1.3. Spit head growth as proxy for hydrodynamic longshore transport

Spit head growth was used as a proxy for net longshore transport. Furthermore, this research was limited to approximating hydrodynamic longshore transport, which was thereafter compared to spit head growth.

Volume changes of the supra-tidal zones signal aeolian forcing causes significant volume changes on the PHSD. The total eroded volume of the supra-tidal zone is comparable to that of total volume losses on the intertidal zone.

Only considering hydrodynamic longshore transport is hypothesized to have the limitation of underestimating the total sand transport on the PHSD. Considering the dominant wind direction to be Southwest, it is expected that spit growth is partially the result of aeolian transport.

8.2. Review on model study results

Prior to construction, a model study was performed by (Witteveen+Bos, 2016) to assess the morphological stability of the PHSD. The study evaluated the morphological development of the project by conducting a 5-year simulation, which included both yearly averaged and storm forcing conditions.

To consider year-round and storm conditions, a 'model train' approach was employed. The boundary conditions, such as waves and water levels, were derived from SWAN and DELFT3D model runs. Wave-current interactions are not considered within the model.

Based on observations on morphological development in (Morphology), it is concluded the model study underestimated the growth of the spit head and development of the tidal opening over time. This discrepancy between the model results and measurements is discussed through an assessment of the applicability of some key assumptions that were made in the model study. Differences in model output and on-site measurements is seen in (Figure 8.1).

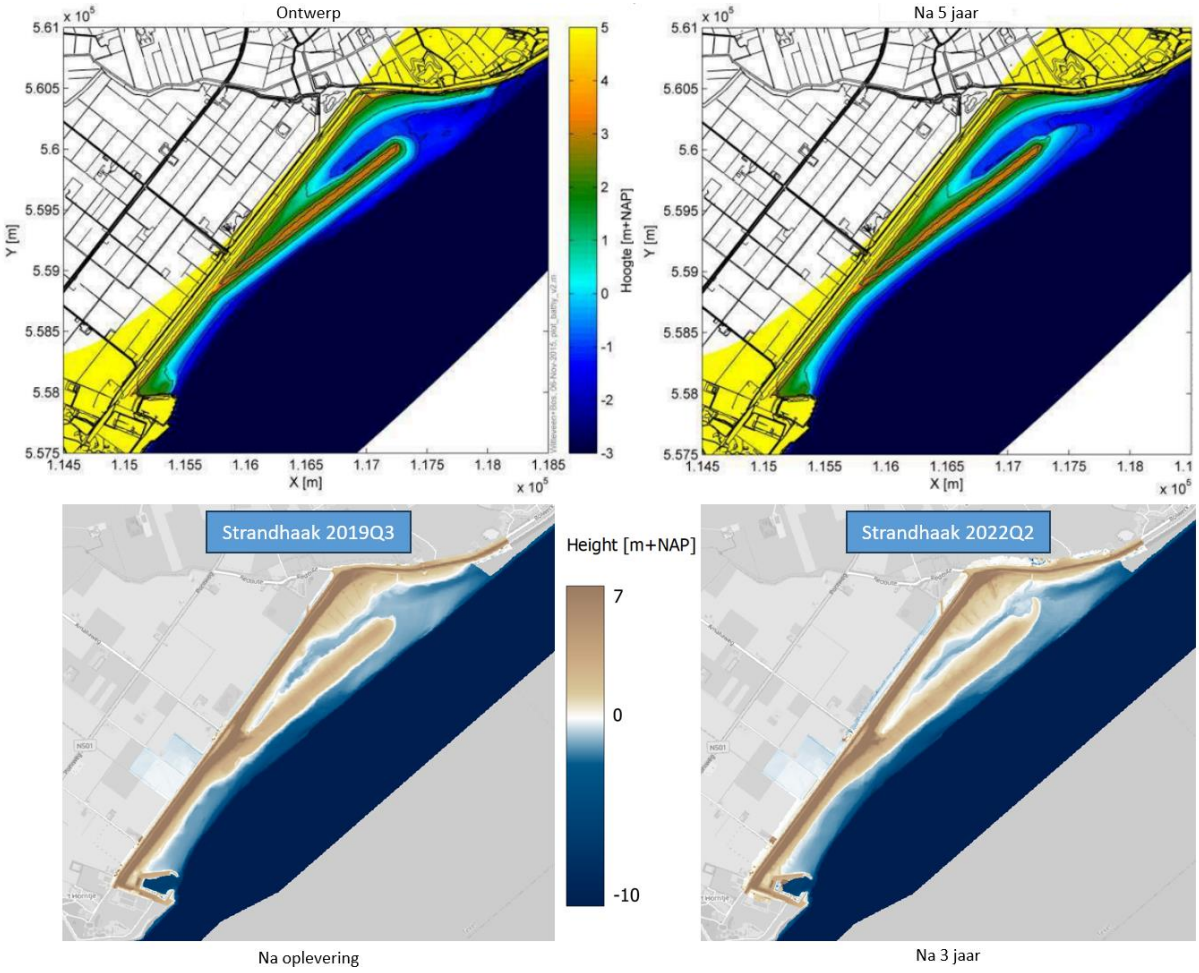

Figure 8.1: Upper left panel) Designed morphological shape of the PHSD. Lower left panel) Actual morphological shape of the PHSD after construction in 2019Q3. Upper right panel) Modelled morphological shape of the PHSD after 5 years of forcing in XBeach. Lower right panel) Actual morphological shape of the PHSD after 4 years of service lifetime.

8.2.1. Spit head growth

Spit head growth narrows the inlet of the tidal lagoon behind, which must remain open for successful development of habitats. To enforce this requirement, one of the key performance indicators is defined as the morphological stability of the tidal opening.

The model study analyzes the tidal opening at a cross-section parallel to the shoreline orientation of the elongated spit (50 degrees North). However, on-site measurements reveal that the growth of the spit head does not occur in the Northeast direction. Instead, it develops in a hook-shape and extends more towards the absolute North. Consequently, the critical cross-section that represents the actual tidal conveyance area after four years of morphological development differs from the cross-section analyzed in the model study. This causes the tidal conveyance area after 5 years of development to be overestimated in the model study.

Uncertainty is expressed regarding the accuracy of the XBeach model regarding magnitude and direction of the spit head growth. To verify this hypothesis, the model results must be examined in more detail. The latter requires an acquisition of the XBeach model and reanalysis of model results.

8.2.2. The effect of wave forcing and set-up/set-down

Water levels for the model study were obtained from a DELFT3D PACE model, which was calibrated to account for tide and wind-induced set-up. However, it should be noted that the model does not

consider the correlation between wind, water levels, and wave conditions for representative yearly conditions.

The justification provided for this assumption is that representing a wide range of water levels, currents, and waves during the simulation is of utmost importance. However, based on the study's results, it is hypothesized that this assumption leads to a combination of forcing conditions that do not occur in reality at the PHSD.

Strong Southwest winds (v_{wind} > 6.0 ms^{-1}) coincide with set-up of the water level (5.3). This results in larger wave heights nearshore as depth-induced breaking on the low-gradient platform is limited. In addition, water level set-up results in decreased refraction of wind waves. Therefore, increased angles of incidence are observed nearshore that result in larger wave induced currents.

The opposite is true for strong Northeast winds that coincide with a set-down of the water level. The corresponding Northeast waves will decrease in height as depth-induced breaking occurs more often. The angle of incidence decreases as refraction is enhanced, which results in decreased wave-induced longshore currents.

By uncoupling wind conditions and water levels, the model overestimates potential transport of Northeast waves while underestimating transport capacity of Southwest waves. The result is an underestimation of spit net Northeastward sediment transport and spit head growth. In conclusion, when modelling morphological development of low-energy beaches, it is important to include water level variations as it coincides with specific combinations of wave conditions, thereby influencing sediment transport and long-term morphological development.

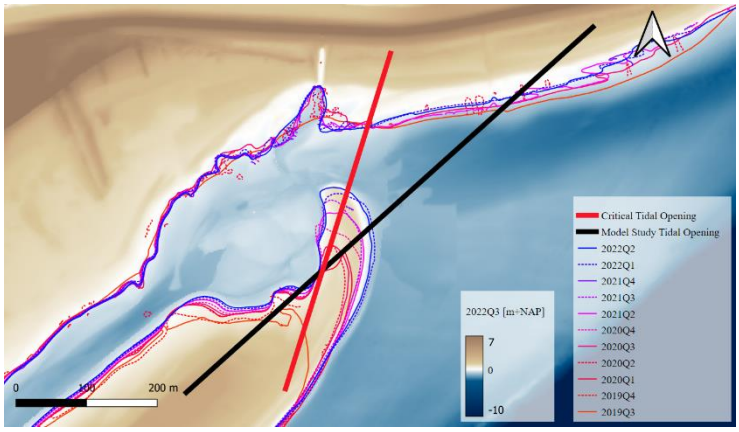

Figure 8.2: Spit head growth indicated by 0.0 m+NAP contour lines demarcating consistent growth of the spit head.

To reduce the computational intensity of model runs, a reduced number of wind conditions is selected in (Witteveen+Bos, 2016). A requirement for the selected conditions is that they are representative of yearly averaged forcing conditions.

As previously mentioned, systematic set-down with Northeast waves, and set-up with Southwest waves is not considered. Therefore, it is likely that the selected set of forcing conditions in the model study may overrepresent Northeasterly waves and underrepresent Southwesterly waves. This emphasizes the importance of considering systematic water level fluctuations, when selecting forcing conditions for low-energy environments.

8.3. Review on literature

A study by (Ton et al., 2023) identifies larger lake-scale currents, observed in the Markermeer, to influence nearshore currents. Large scale currents are even dominant over wave-driven currents for most wind forcing conditions. In addition, local geometric features such as groynes, breakwaters and shoreline changes have been seen to induce smaller scale nearshore circulation cells.

This thesis research differentiates itself from the study by (Ton et al., 2023) as the studied coastline is not situated in a closed lake-environment but in a tidal basin. Large scale currents do prevail, but in the form of tidal currents rushing in and out of the Wadden Sea basin, which are also measured on the low-gradient platform. Nearshore structures such as the NIOZ harbor breakwaters can impose the mentioned nearshore circulation cells altering flow directions and influencing sediment transport directions.

In this research, waves and wave-induced currents have been determined to be the dominant forcing in the surfzone. Large scale tidal currents which are predominantly observed on the low-gradient platform are less pronounced. A possible explanation for this discrepancy is that tidal currents at the PHSD might be weaker than the described large-scale lake circulation currents in the Markermeer. Another explanation could be that waves on the PHSD are simply more energetic. Lastly, the importance of local geometrical features or orientation of the studied coastline causes differences that are essential for bringing offshore currents nearshore.

have been determined to be the dominant forcing mechanism dictating both sediment transport magnitude and direction during most forcing conditions. Note that this conclusion was derived based on conditions for the elongated spit, which is the most wave exposed stretch of coastline within the studied coastline. The role of waves is likely to be less influential near the NIOZ harbor due to less wave exposure.

Large scale currents and nearshore circulation cells might be more influential for development of areas closer to the NIOZ harbor, as wave exposure is limited, and more complicated flow patterns might arise.

9. Conclusion

This section concludes on the main findings from Chapter 4, 5 and 6 and Chapter 7 and provides answers to the sub research questions presented in (2.1). The main research question will be answered by answering the four sub questions.

Main research question

What is the role of different hydrodynamic forces and how does it influence morphology on the Prins Hendrik Sand Dike?

9.1. Sub question 1: Literature review

Which hydrodynamic processes are influential for development of low-energy beaches based on literature?

The Prins Hendrik Sand Dike has been defined as a sandy beach in a low-energy tidal environment, placed in a non-equilibrium orientation with respect to the dominant wind-direction. In this context, general information on low-energy beaches and their behavior and forcings was deemed applicable.

The main forcing mechanism of low-energy beaches is wind forcing. This creates wind waves, wind-induced currents, and water level fluctuations, which are all deemed influential for morphological development of low-energy beaches. Wind waves experience limited refraction on the low-gradient platform and reach the shoreface under high angles which causes enlarged longshore sediment transport rates (Jackson et al., 2002). Frequency and intensity of storm events determine the long-term evolution of low-energy beaches. Mild and infrequent storms result in quasi-stable low-energy beaches while energetic and frequent storms result in structurally eroding 'storm-relict' beaches (Fellowes et al., 2021). During such storms, the combination of increased water levels coinciding with large waves can cause severe erosion (kirk et al. 2000). In contrast to exposed beaches, low-energy beaches are not reshaped by milder waves as wave energy during such conditions is not sufficient.

9.2. Sub question 2: Morphologic development

What has been the morphologic response of the studied coastline under episodic and average forcing conditions?

Morphologic development of the coastal cross-profile is limited to periods of energetic wind forcing coinciding with increased nearshore wave heights. Redistribution of sediment from the upper shoreface to the lower shoreface was observed. Moreover, the magnitude of the sediment redistribution was found to be correlated with local wave exposure. In other words, areas that were more exposed to Southwest waves, such as the elongated spit section, experienced a significantly larger volume of sediment redistribution compared to the sheltered harbor section, where the shoreface is not altered as a result of energetic conditions.

The long-term development of the studied coastline is analysed for three different sections of the PHSD; the NIOZ harbor section, the elongated spit, and the spit head. The spit head is consistently increasing in volume resulting in growth of the spit head towards the North. Volume increase is observed in both summer and winter periods. Furthermore, spit head growth shows no sign of reduction over time. Sudden jumps in spit head growth do occur coinciding with increased storm intensity and frequency.

Volume changes of the elongated spit signal storm driven development. Erosion of the shoreface only occurs during the winters of 2019-2020 and 2021-2022. Summers and winters with

reduced storm intensity do not result in erosion of the shoreface. Slight accretion of the shoreface after storm events does occur, hinting limited rebuilding capacity is possible but limited.

The NIOZ harbor section faces structural erosion. This section is not storm-driven, but experiences constant volume decrease of the shoreface in both summer and winter periods. The volume decrease is seen within cross-shore profile as general shoreline retreat and a steepening of the shoreface. This section has a primary function as defense and must be maintained if erosion continuous

9.3. Sub question 3: Hydrodynamic drivers

'What are the main drivers of morphologic development and how do they influence the morphology of the studied coastline?'

The difference in wave exposure during Southwest storm conditions is significant. Wave heights on the exposed elongated spit are on average twice as high as observed near the sheltered NIOZ harbor. Wave-energy, being related to wave height squared, is therefore approximately 4 times higher at the exposed elongated spit with respect to the sheltered NIOZ-harbor.

Waves can break on the low-gradient platform as a result of low water levels coinciding with high wave heights. A breaker parameter of 0.48 was derived during the Southwest storm. Wave breaking on the low-gradient platform causes waves approaching the shoreface to be limited in height. This causes wave-energy to be reduced before waves approach the steep foreshore, where most longshore transport of sediment is expected.

Mean currents on the low-gradient platform are a combination of tide- and wind-driven flow. Mean currents at the shoreface are a combination of tide-, wind- and wave-driven flow. Increased wind forcing during the Southwest storm seen in the SEDMEX campaign causes mean currents on the elongated spit to be enhanced in flood direction and reduced in ebb-direction during Northeast winds. Wind forcing from the Southwest is capable of reversing ebb-tidal flow entirely when wind velocities increase above 7 ms^{-1}, based on a conceptual model for the influence of wind on tidal currents. Lastly, tidal- and wind-driven flow are reduced 40% near the steep shoreface as a result of increased friction. Wave-driven currents are dominant within the surfzone.

During calm conditions (v_{wind} < 6.0 ms^{-1}), the occurrence of significant near bed orbital flow is limited due to small wave heights. Increased near bed orbital flow is only observed for brief moments around low water, coinciding with slack water conditions. Under these circumstances, the fine sand fraction of the sediment composition is mobilized but with limiting flow velocities transport is negligible.

At the shoreface, the energy carried by the small waves is dissipated near the waterline. This wave energy dissipation occurs over the tidal water level range but is more concentrated at high and

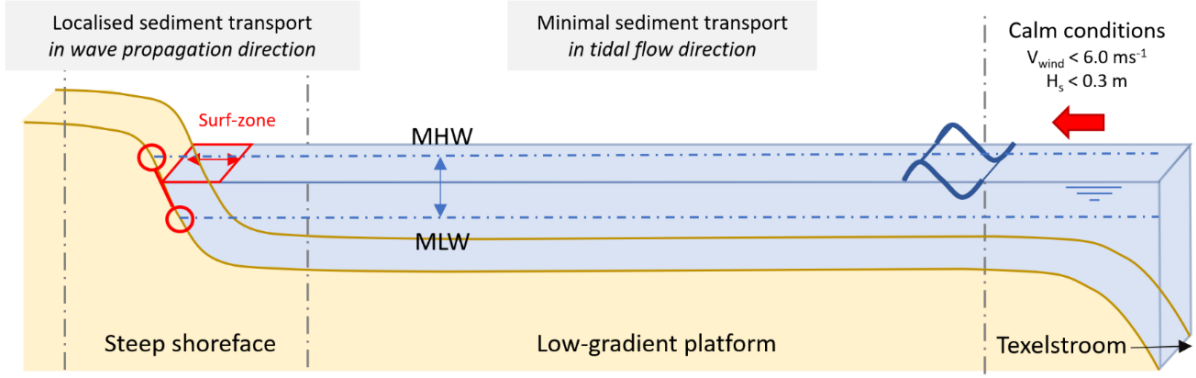

Figure 9.1: Summary of the findings regarding calm conditions forcing the PHSD.

low water levels due to an extended exposure period. Wave breaking facilitates continuous but limited in magnitude sediment transport in wave propagation direction.

Energetic conditions (v_{wind} > 6.0 ms^{-1}) cause sediment to be mobilized more often. As the overall ratio wave height to depth is increased, near bed orbital motion causes the maximum bed shear stresses to be sufficiently large for exceedance of critical shear stresses during the larger part of the tidal cycle around low-water. Bed shear stresses indicate bed-load transport over rippled bed to be the dominant mode of sediment transport both on the low-gradient platform and on the steep shoreface.

Wave properties quickly adapt to wind forcing conditions resulting in increased wave heights to occur simultaneously with increased wind velocity. The increased wind velocity has noticeable effects on the flow patterns on the low-gradient platform. The SW wind causes flood flow enhancement and reduced ebb flow. This influences sediment transport for prevalent Southwest storms to be mainly directed in flood direction (coinciding with wind and wave directions).

Within the surfzone near the steep shoreface, wave energy is dissipated, and sediment mobilization is assumed largest due to the resulting turbulent water motion. Here, a significant increase in flow velocity is observed in the direction of wave propagation resulting from longshore radiation stresses. Ultimately, this enhances sediment transport in flood direction (towards the Northeast).

The interactions between wind, waves, and bed shear stresses all support the conclusion that waves are the dominant forcing mechanism. Wind waves mobilize the sediment while both wind and waves enhance mean currents. The latter causes sediment transport on the low-gradient platform and the steep shoreface to be in flood direction on average.

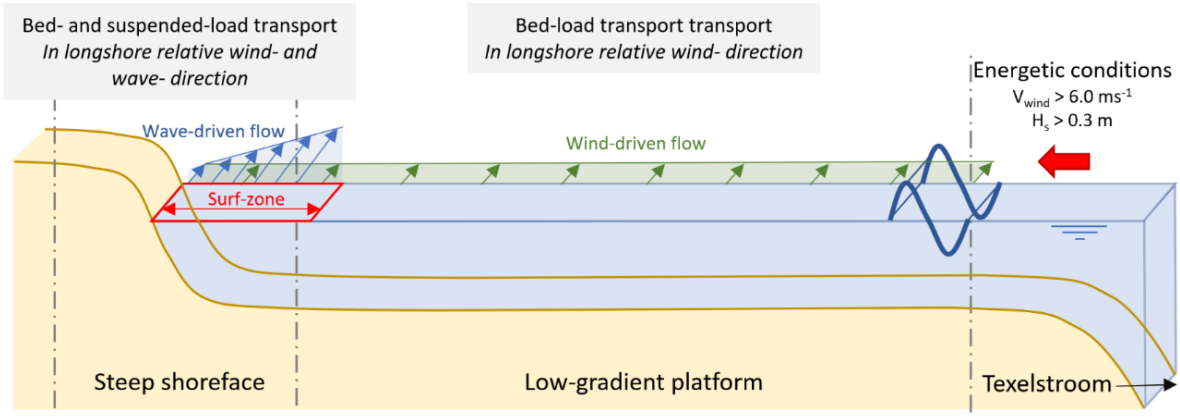

Figure 9.2: Summary of the findings regarding energetic conditions forcing the PHSD.

9.4. Sub question 4: Longshore transport

'Can the forcing climate and longshore transport rates be approximated effectively using simple engineering formulae?'

Forcing conditions are hindcasted and validated to on-site measurements. Wave and current properties could now be hindcasted for the full service-lifetime of the PHSD and longshore transport was approximated using established engineering formulae. Cumulative longshore transport shows a similar signature as spit head growth. Moments of increased erosion of the elongated spit and simultaneous accretion of the spit head align with increased net longshore transport of sediment towards the Northeast (2019Q4-2020Q1).

A difference between simulated and observed spit head growth is that simulated spit head growth shows distinct periods of net Southwest ward transport of sediment. This means the spit head could at

times erode and decrease in volume. This is however not seen from drone data, which suggests a continuous accretion of the spit head.

The morphological climate indicates that the interconnectivity of wave conditions and water level set-up / set-down plays an important role in morphological development. Strong easterly winds do not result in significant sediment transport as waves break on the low-gradient platform before they reach the morphologically active steep foreshore. This finding highlights the importance of considering interconnectivity of waves and water levels during modelling efforts.

Bosboom, J., & Stive, M. J. F. (n.d.). Coastal Dynamics. *2021*. https://doi.org/10.5074/T.2021.001

Brand, E. (n.d.). *Erosion and transport of sediment and channel-shoal sediment exchange at a shoal in the Western Dutch Wadden Sea*.

Castelle, B., Ritz, A., Marieu, V., Nicolae Lerma, A., & Vandenhove, M. (2022). Primary drivers of multidecadal spatial and temporal patterns of shoreline change derived from optical satellite imagery. *Geomorphology*, *413*. https://doi.org/10.1016/j.geomorph.2022.108360

Colosimo, I., de Vet, P. L. M., van Maren, D. S., Reniers, A. J. H. M., Winterwerp, J. C., & van Prooijen, B. C. (2020a). The impact of wind on flow and sediment transport over intertidal flats. *Journal of Marine Science and Engineering*, *8*(11), 1–26. https://doi.org/10.3390/jmse8110910

Colosimo, I., de Vet, P. L. M., van Maren, D. S., Reniers, A. J. H. M., Winterwerp, J. C., & van Prooijen, B. C. (2020b). The impact of wind on flow and sediment transport over intertidal flats. *Journal of Marine Science and Engineering*, *8*(11), 1–26. https://doi.org/10.3390/jmse8110910

de Vet, P. L. M., van Prooijen, B. C., Schrijvershof, R. A., van der Werf, J. J., Ysebaert, T., Schrijver, M. C., & Wang, Z. B. (2018). The Importance of Combined Tidal and Meteorological Forces for the Flow and Sediment Transport on Intertidal Shoals. *Journal of Geophysical Research: Earth Surface*, *123*(10), 2464–2480. https://doi.org/10.1029/2018JF004605

Fellowes, T. E., Vila-Concejo, A., Gallop, S. L., Schosberg, R., de Staercke, V., & Largier, J. L. (2021). Decadal shoreline erosion and recovery of beaches in modified and natural estuaries. *Geomorphology*, *390*. https://doi.org/10.1016/j.geomorph.2021.107884

Fokke, L. D. (2021). *Faculteit Civiele Techniek en Geowetenschappen Morfologische analyse strandhaak Prins Hendrikzanddijk*.

Hegge, B., Eliot, I., & Hsu, J. (1996). Sheltered Sandy Beaches of Southwestern Australia. In *Source: Journal of Coastal Research* (Vol. 12, Issue 3).

Hendrik Sanddike Author, P., & Bert Woerdman, J. (2022). *Alongshore variability in hydrodynamics and its implications for sand transport in front of the*.

Hoegen, R. (2022). *Initial erosion-deposition patterns in a sheltered coastal environment: the role of wind, waves, tides and graded sediment*.

Holthuijsen, L. H. (2007). *Waves in Oceanic and Coastal Waters*.

Hopkins, J., Elgar, S., & Raubenheimer, B. (2017). Flow separation effects on shoreline sediment transport. *Coastal Engineering*, *125*, 23–27. https://doi.org/10.1016/j.coastaleng.2017.04.007

Jackson, N. L., & Nordstrom, K. F. (1992). Site Specific Controls on Wind and Wave Processes and Beach Mobility on Estuarine Beaches in New Jersey, U.S.A. In *Source: Journal of Coastal Research* (Vol. 8, Issue 1). Winter. https://www.jstor.org/stable/4297955

Jackson, N. L., Nordstrom, K. F., Eliot, I., & Masselink, G. (2002). *"Low energy" sandy beaches in marine and estuarine environments: a review*. www.elsevier.com/locate/geomorph

Kahma, K., & Calkoen, C. J. (1992). 1520-0485-1520-0485_1992_022_1389_rditog_2_0_co_2. *Journal of Physical Oceanography*, *22*, 1–17.

Klein Obbink, M. (2021). *Multi-fraction sediment sorting and entrainment at the Prins Hendrikzanddijk*.

Mil-Homens, J., Ranasinghe, R., van Thiel de Vries, J. S. M., & Stive, M. J. F. (2013). Re-evaluation and improvement of three commonly used bulk longshore sediment transport formulas. *Coastal Engineering*, *75*, 29–39. https://doi.org/10.1016/j.coastaleng.2013.01.004

Perk, L., van Rijn, L., Koudstaal, K., & Fordeyn, J. (2019). A rational method for the design of sand dike/dune systems at sheltered sites; Wadden Sea Coast of Texel, The Netherlands. *Journal of Marine Science and Engineering*, *7*(9). https://doi.org/10.3390/jmse7090324

Roelvink, D., Huisman, B., Elghandour, A., Ghonim, M., & Reyns, J. (2020). Efficient Modeling of Complex Sandy Coastal Evolution at Monthly to Century Time Scales. *Frontiers in Marine Science*, *7*. https://doi.org/10.3389/fmars.2020.00535

Soulsby, R. (1997). *Dynamics of marine sands A manual for practical applications*. http://www.t-telford.co.uk

Strypsteen, G., van Rijn, L. C., Hoogland, M. D., Rauwoens, P., Fordeyn, J., Hijma, M. P., & Lodder, Q. J. (2021). Reducing aeolian sand transport and beach erosion by using armour layer of coarse materials. *Coastal Engineering*, *166*. https://doi.org/10.1016/j.coastaleng.2021.103871

Ton, A. M., Vuik, V., & Aarninkhof, S. G. J. (2021). Sandy beaches in low-energy, non-tidal environments: Linking morphological development to hydrodynamic forcing. *Geomorphology*, *374*. https://doi.org/10.1016/j.geomorph.2020.107522

Ton, A. M., Vuik, V., & Aarninkhof, S. G. J. (2023). Longshore sediment transport by large-scale lake circulations at low-energy, non-tidal beaches: A field and model study. *Coastal Engineering*, *180*. https://doi.org/10.1016/j.coastaleng.2022.104268

Travers, A. (2007). Low-energy beach morphology with respect to physical setting: A case study from Cockburn Sound, Southwestern Australia. *Journal of Coastal Research*, *23*(2), 429–444. https://doi.org/10.2112/04-0275.1

van Alphen, J., Haasnoot, M., & Diermanse, F. (2022). Uncertain Accelerated Sea-Level Rise, Potential Consequences, and Adaptive Strategies in The Netherlands. *Water (Switzerland)*, *14*(10). https://doi.org/10.3390/w14101527

Van Rijn, L. C. (2014). A simple general expression for longshore transport of sand, gravel and shingle. *Coastal Engineering*, *90*, 23–39. https://doi.org/10.1016/j.coastaleng.2014.04.008

Wellen, F. W. (2021). *Development of a non-equilibrium beach in a low-energy lake environment Using the Noordstrand of the Marker Wadden as a case study*.

Witteveen+Bos. (2016). *PHZD Morfologische Studie*.

Woerdman, J. B. (2022). *Alongshore variability in hydrodynamics and its implications for sand transport in front of the*.

Wright, L. D., & Short, A. D. (1984). MORPHODYNAMIC VARIABILITY OF SURF ZONES AND BEACHES: A SYNTHE:~IS*. In *Marine Geology* (Vol. 56).

Wu, J. (1982). Wind-stress coefficients over sea surface from breeze to hurricane. *Journal of Geophysical Research*, *87*(C12), 9704. https://doi.org/10.1029/jc087ic12p09704

Appendix A: Cross-shore profile development Transect 6

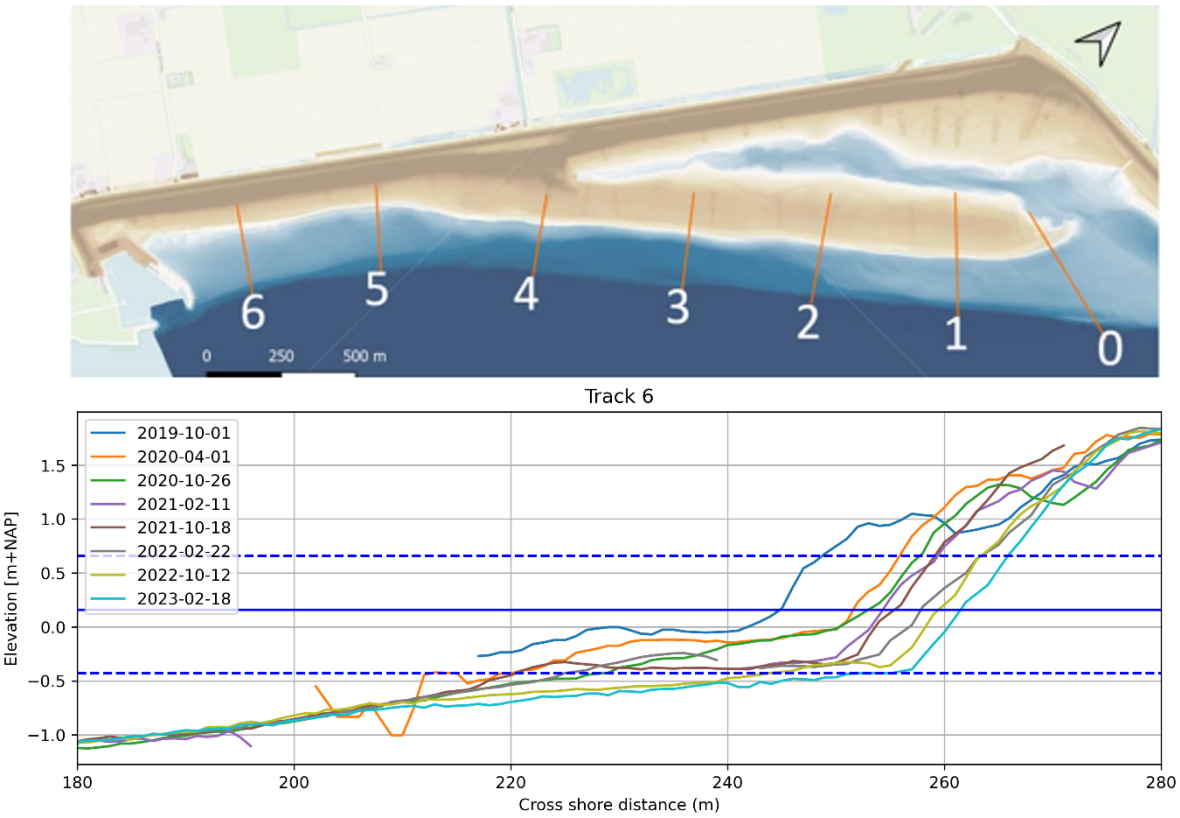

Figure 0.1: Upper panel) Map view of PHSD and position and numbering of transects. Lower panel) Cross shore bed profile development of transect 6 during 3.5 years of service-lifetime (near the NIOZ harbor) using GPS data.

Appendix B: Cross-shore profile development (episodic)

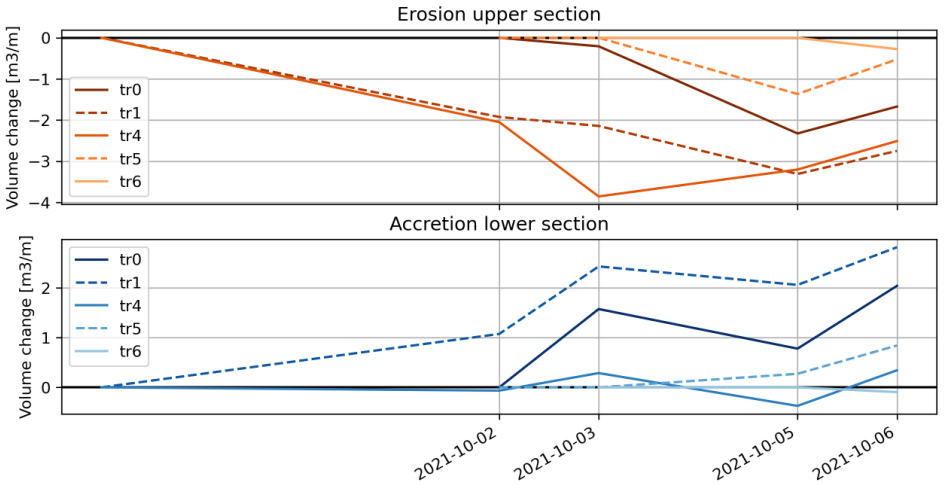

Figure 0.1: Net volume changes of the upper and lower section during the storm period (between 28th of September and 6th of October) along the studied coastline derived from GPS measurements.

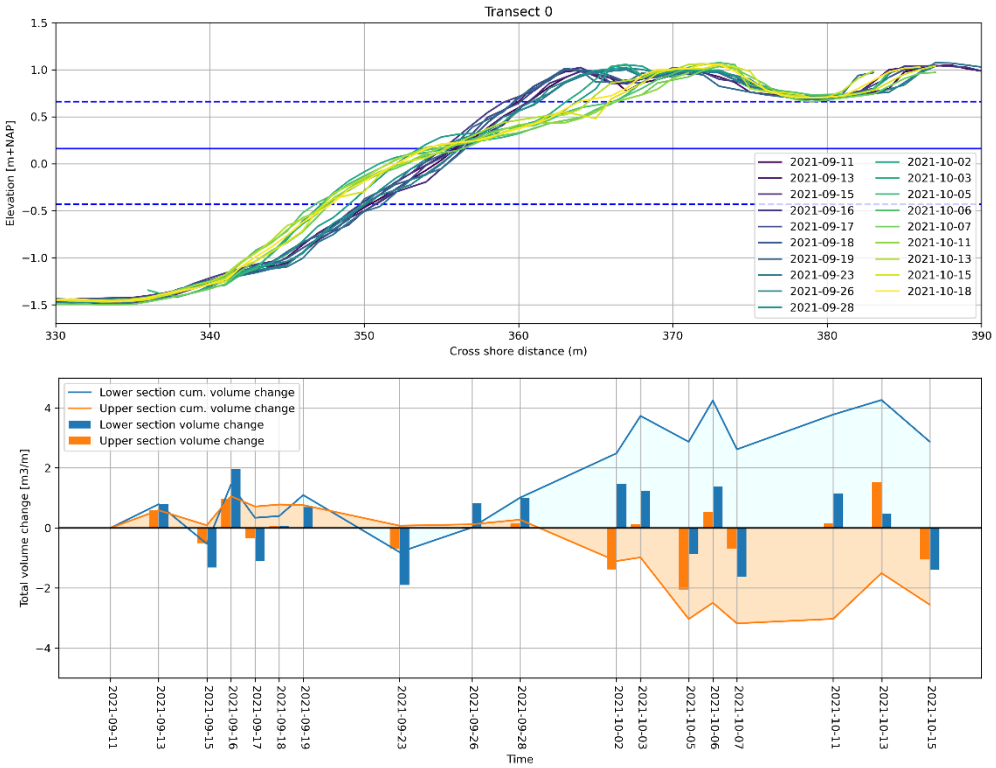

Figure 0.2: Upper panel) Map view of PHSD and position and numbering of transects. Lower panel) Cross shore bed profile development of transect 6 during 3.5 years of service-lifetime (near the NIOZ harbor) using GPS data.

Appendix C: Summary of hydrodynamic conditions (SEDMEX)

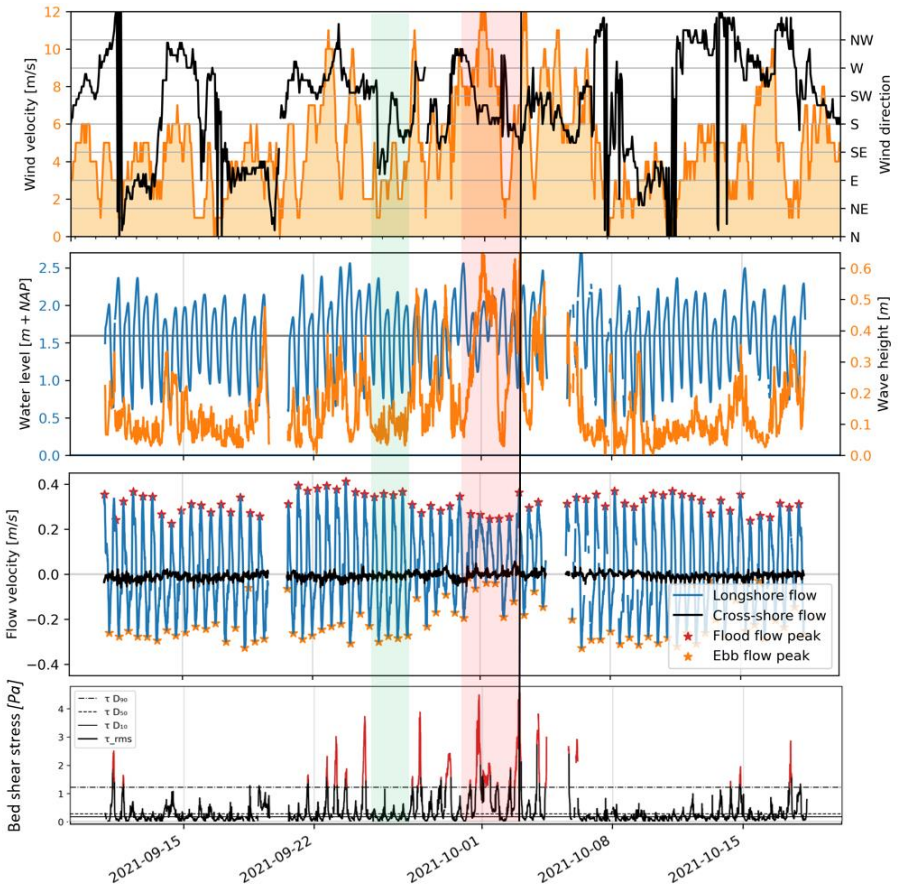

Figure 0.1: Summary of wind forcing (upper panel), wave and water levels (upper-middle panel), longshore and cross-shore flow velocity (lower-middle panel), and root-mean squared bed shear stresses (lower panel). Green shaded area corresponds to the 'calm period' elaborated in (5.4.2). Red shaded area corresponds to the 'energetic period' elaborated in (5.4.3).

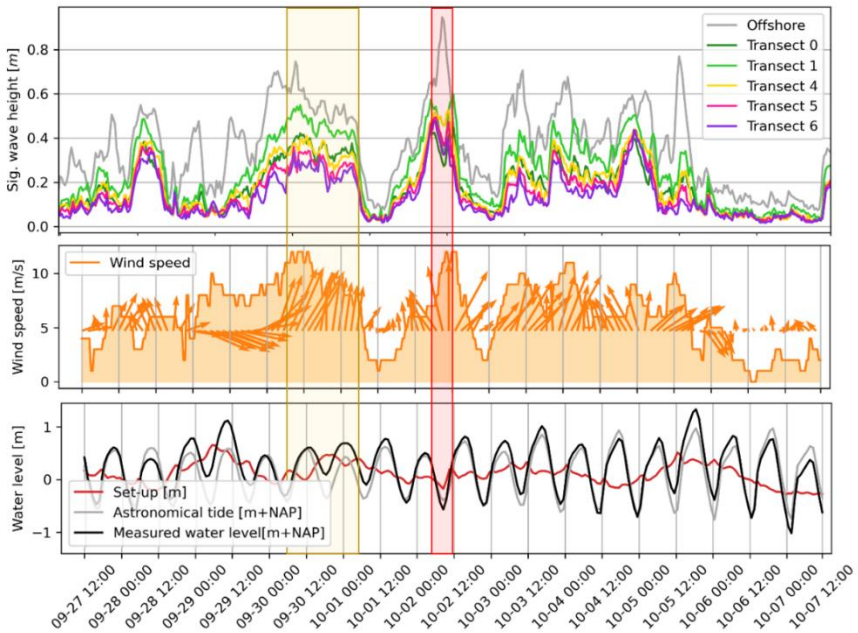

Figure 0.4: Upper panel, Significant wave height measured by OSSI's placed along the studied coastline. Middle panel, corresponding wind conditions (vectors are not linked to the y-axis). Lower panel, water level conditions retrieved from Oudeschild measuring station.

Appendix D: Effect of wind on tidal flow on the low-gradient platform

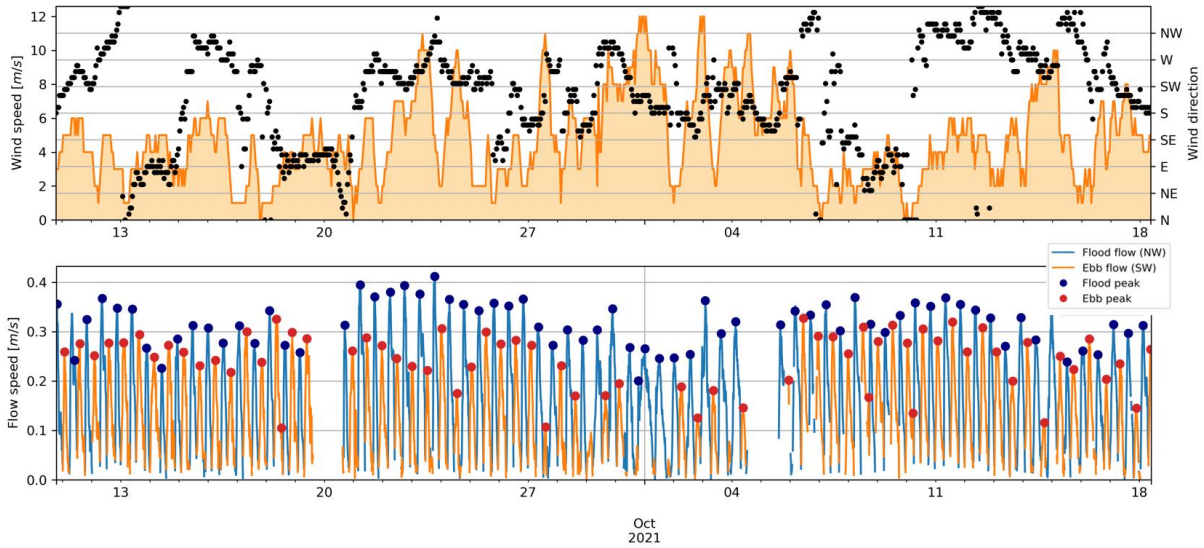

Figure 0.1: Summary of wind forcing (upper panel), wave and water levels (upper-middle panel), longshore and cross-shore flow velocity (lower-middle panel), and root-mean squared bed shear stresses (lower panel). Green shaded area corresponds to the 'calm period' elaborated in (5.4.2). Red shaded area corresponds to the 'energetic period' elaborated in (5.4.3).

Appendix E: Cross-shore variation in currents

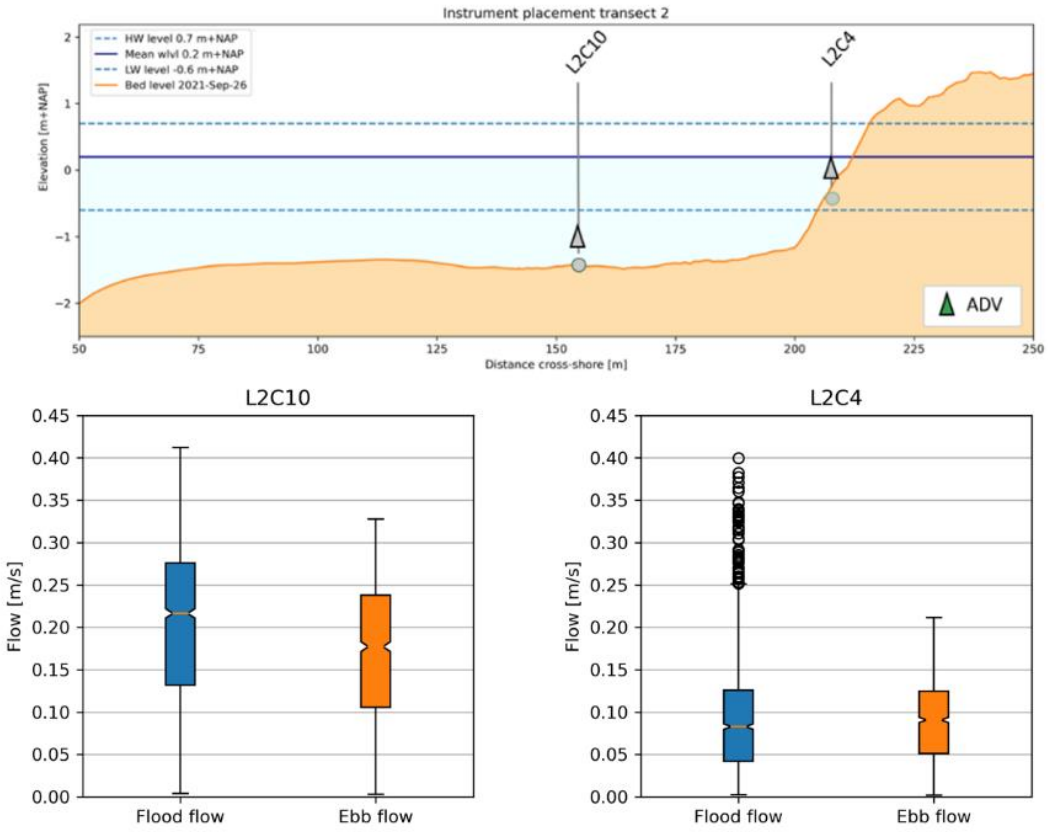

Figure 0.1: Upper panel, placement of L2C10 and L2C04 on the low-gradient platform on the elongated spit (transect 1). lower panels, flood- and ebb-current statistics during SEDMEX.

Appendix F: Validation offshore wave simulation

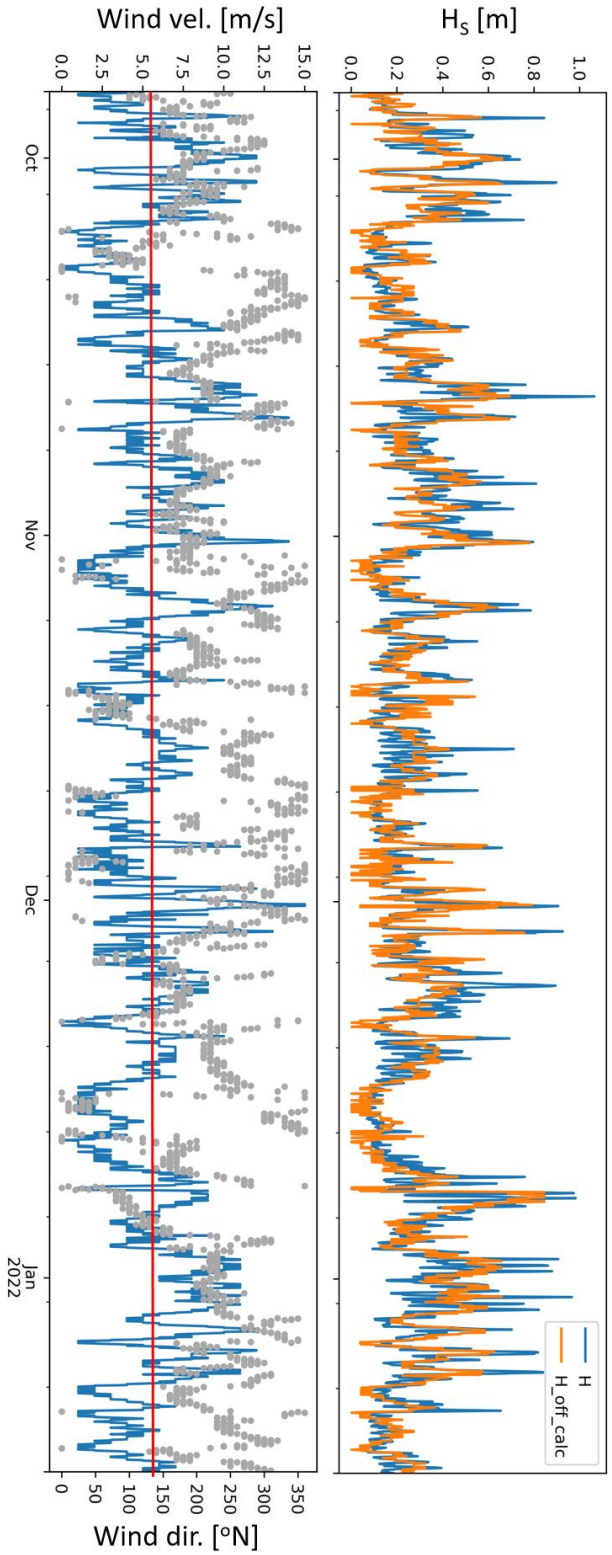

Figure 0.1: Right panel) Time-series of offshore significant wave height measured by the Xylem wave buoy deployed between October 2021 and January 2022 (blue line) and the simulated offshore wave height (orange line) following the procedure described in (6.1.1). Left panel) Wind velocity (blue line) and direction (gray dots) measured at 'de Kooij' measuring station (2.2.3) during the Xylem measuring period.

Appendix G: Validation offshore wave simulation (zoom-in)

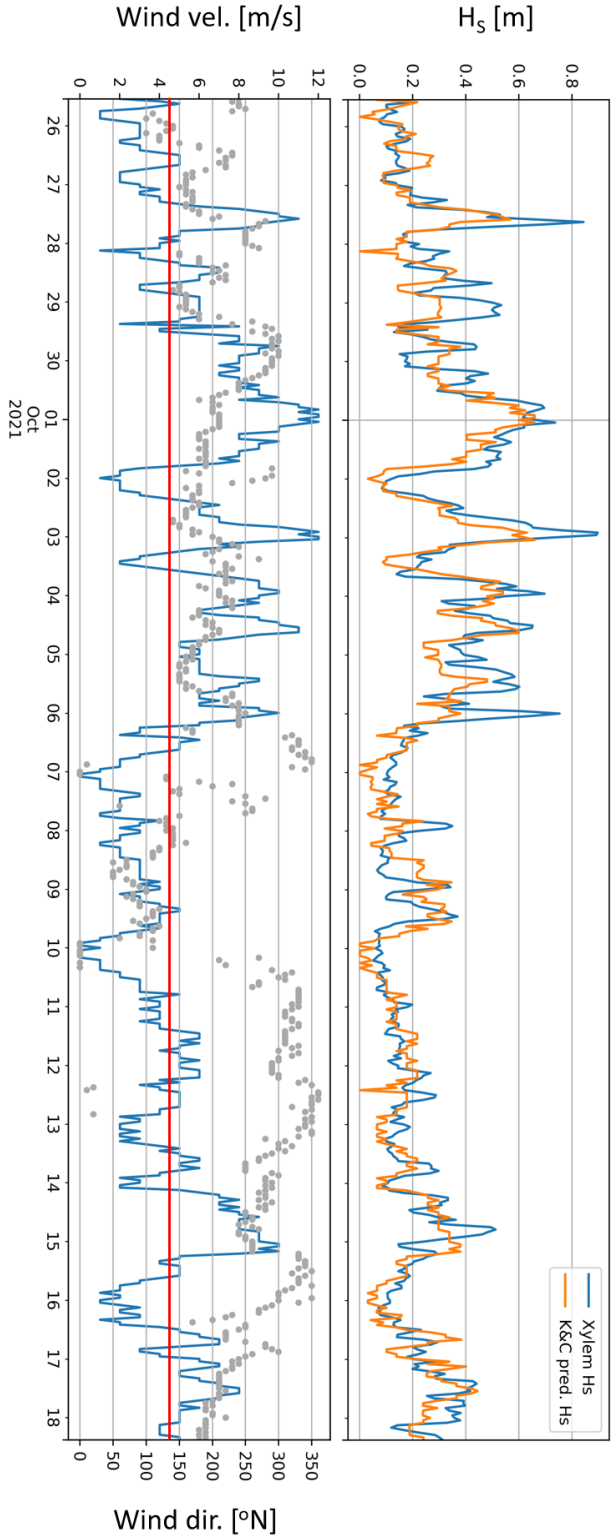

Figure 0.1: Right panel) Zoomed-in time-series of offshore significant wave height measured by the Xylem wave buoy during stormy conditions around 2nd of October 2021 (blue line) and the simulated offshore wave height (orange line) following the procedure described in (6.1.1). Left panel) Wind velocity (blue line) and direction (gray dots) measured at 'de Kooij' measuring station (2.2.3).

Appendix H: Validation nearshore wave simulation

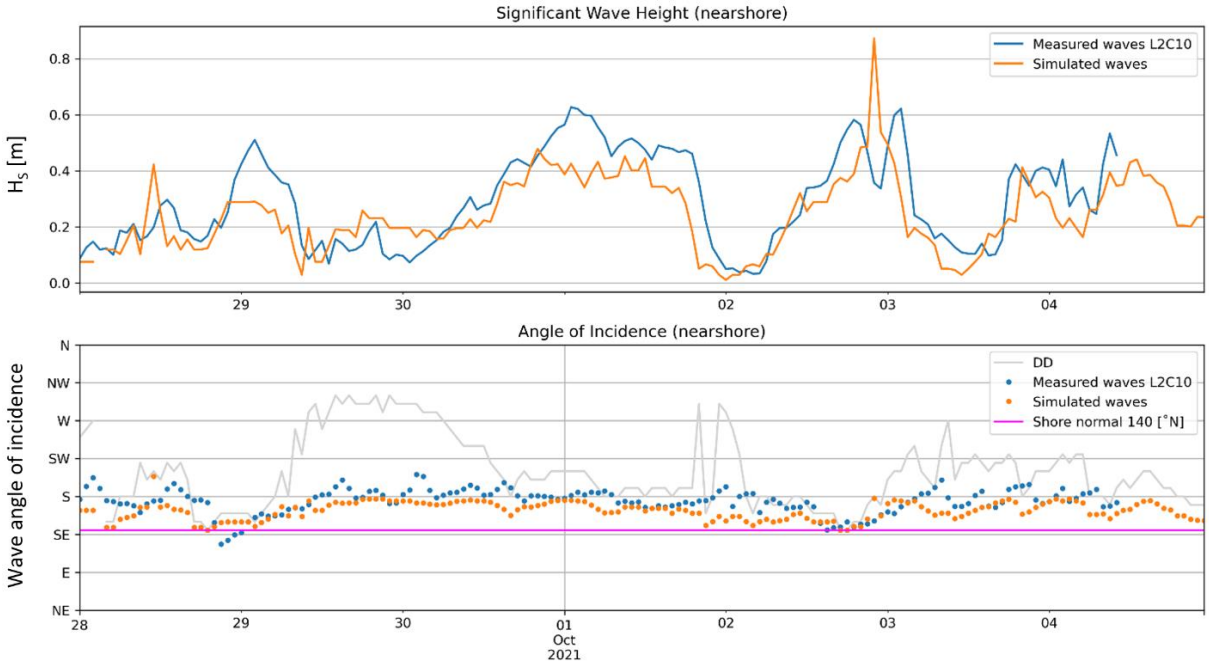

Figure 0.1: Upper panel) Nearshore measured significant wave height at L2C10 during the SEDMEX campaign (blue line) and nearshore simulated significant wave height (orange line) based on the procedure in (). Lower panel) Wave angle of incidence measured (blue dots) and simulated (orange dots), the gray line represents wind direction measured at 'de Kooij' measuring station.